

1 **Holocene atmospheric circulation in the central North Pacific: a new terrestrial**
2 **diatom and $\delta^{18}\text{O}$ dataset from the Aleutian Islands**

3

4 Hannah L Bailey ^{a,b,*}, Darrell S Kaufman ^c, Hilary J Sloane ^d, Alun L Hubbard ^{e,f}, Andrew
5 CG Henderson ^g, Melanie J Leng ^{d,h}, Hanno Meyer ^b, and Jeffrey M Welker ^a

6

7 ^a Department of Biological Sciences, University of Alaska Anchorage, Anchorage, AK 99508, USA

8 ^b Alfred Wegener Institute for Polar and Marine Research, Potsdam 14473, Germany

9 ^c School of Earth Sciences & Environmental Sustainability, Northern Arizona University, Flagstaff, AZ 86011,
10 USA

11 ^d NERC Isotope Geosciences Facility, British Geological Survey, Nottingham NG12 5GG, UK

12 ^e Centre for Arctic Gas Hydrate, Environment and Climate, Department of Geology, UiT The Arctic University
13 of Norway, 9037 Tromsø, Norway

14 ^f Institute of Geography & Earth Sciences, Aberystwyth University, Aberystwyth SY23 3DB, UK

15 ^g School of Geography, Politics and Sociology, Newcastle University, Newcastle-upon-Tyne, NE7 1RU, UK

16 ^h Centre for Environmental Geochemistry, School of Biosciences, University of Nottingham, Loughborough,
17 LE12 5RD, UK

18 * *Corresponding author*. Email address: hannah.bailey@oulu.fi

19

20 *Key words:* Holocene; Paleoclimate; North Pacific; Limnology; Stable Isotopes; Diatoms

21

22 *Highlights:*

- 23 ▪ New Holocene oxygen isotope record from the Aleutian Islands
- 24 ▪ Diatom $\delta^{18}\text{O}$ reflects shifts in synoptic-scale atmospheric circulation
- 25 ▪ Warmer/wetter early-mid Holocene, cooler/drier after 4.5 ka
- 26 ▪ Enhanced winter circulation corresponds to Holocene glacier advances
- 27 ▪ Current environmental changes unprecedented within past 9.6 ka

28 **Abstract**

29 The North Pacific is a zone of cyclogenesis that modulates synoptic-scale atmospheric
30 circulation, yet there is a paucity of instrumental and paleoclimate data to fully constrain its
31 long-term state and variability. We present the first Holocene oxygen isotope record
32 ($\delta^{18}\text{O}_{\text{diatom}}$) from the Aleutian Islands, using siliceous diatoms preserved in Heart Lake on
33 Adak Island (51.85° N, 176.69° W). This study builds on previous work demonstrating that
34 Heart Lake sedimentary $\delta^{18}\text{O}_{\text{diatom}}$ values record the $\delta^{18}\text{O}$ signal of precipitation, and correlate
35 significantly with atmospheric circulation indices over the past century. We apply this
36 empirical relationship to interpret a new 9.6 ka $\delta^{18}\text{O}_{\text{diatom}}$ record from the same lake,
37 supported by diatom assemblage analysis. Our results demonstrate distinct shifts in the
38 prevailing trajectory of storm systems that drove spatially heterogeneous patterns of moisture
39 delivery and climate across the region. During the early-mid Holocene, a warmer/wetter
40 climate prevailed due to a predominantly westerly Aleutian Low that enhanced advection of
41 warm ^{18}O -enriched Pacific moisture to Adak, and culminated in a $\delta^{18}\text{O}_{\text{diatom}}$ maxima (33.3 ‰)
42 at 7.6 ka during the Holocene Thermal Maximum. After 4.5 ka, relatively lower $\delta^{18}\text{O}_{\text{diatom}}$
43 indicates cooler/drier conditions associated with enhanced northerly circulation that persisted
44 into the 21st century. Our analysis is consistent with surface climate conditions inferred from
45 a suite of terrestrial and marine climate-proxy records. This new Holocene dataset bridges the
46 gap in an expanding regional network of paleoisotope studies, and provides a fresh
47 assessment of the complex spatial patterns of Holocene climate across Beringia and the
48 atmospheric forces driving them.

49

50

51

52

53

54 **1. Introduction**

55 Numerous paleoenvironmental studies now contribute to a global synthesis and
56 understanding of Holocene climate change over the past 11.7 ka [*Mayewski et al.* 2004;
57 *Marcott et al.* 2013; *Rehfeld et al.* 2018]. By comparing common trends between individual
58 proxy records, these studies provide a means to infer the timing, scale, and spatial extent of
59 major Holocene climatic features. These include stepwise climate transitions, intervals
60 exceeding twentieth century warmth, and the low-frequency behaviour and modes of natural
61 climate variability. At broad (i.e. global) spatial and temporal scales these trends are
62 relatively coherent and unambiguous, yet at finer spatial scales, climate variability is more
63 pronounced due to local and regional factors. Such variability is highlighted in two recent
64 paleoclimate syntheses focused on west and eastern Beringia – the region extending from
65 northeast Siberia to northwest Canada (Fig. 1a) [*Brooks et al.* 2015; *Kaufman et al.* 2016].
66 While general circulation models (GCM) typically emphasise insolation as the key driver of
67 millennial-scale Holocene climate change [*Renssen et al.* 2009], these compilations indicate a
68 more complex and spatially heterogeneous climate evolution than implied by linear insolation
69 forcing alone. For example, major climatic features previously considered ubiquitous, such as
70 a prominent Holocene thermal maximum (HTM) [*Kaufman et al.* 2004], are now recognised
71 to be spatially asynchronous across this vast region [*Kaufman et al.* 2016]. Moreover,
72 existing terrestrial water isotope records are also shown to be ambiguous and contradictory
73 during the Holocene [*Kaufman et al.* 2016] and the most recent suite of model-data
74 comparisons reveal significant mismatches between simulated and reconstructed Holocene
75 temperatures in Alaska [*Zhang et al.* 2017].

76 At a synoptic scale, Beringia is located within the main centre of influence of the
77 Aleutian Low, one of the most dominant ocean-atmospheric systems in the Northern
78 Hemisphere with global climatic significance [*Rodionov et al.* 2007]. However, virtually all
79 available terrestrial paleoclimate data are restricted to mainland Alaska and eastern Russia

80 [Sundqvist *et al.* 2014; Brooks *et al.* 2015; Kaufman *et al.* 2016], and compared to lower
81 latitude regions, paleoisotope reconstructions are sparse [Kaufman *et al.* 2016]. This partly
82 reflects a lack of base-line water isotope measurements for constraining the regional water
83 isotope cycle [e.g. Welker, 2000; Anderson *et al.* 2016], as well as a paucity of lake core
84 studies with continuous sequences of carbonate-rich sediments – or suitable alternatives – for
85 isotopic analysis. Hence, to elucidate past and future climate in this region, there is an
86 outstanding requirement for greater spatial coverage of highly resolved and accurately dated
87 paleoclimate datasets, as well as an empirical-based understanding of the atmospheric and
88 environmental controls driving them.

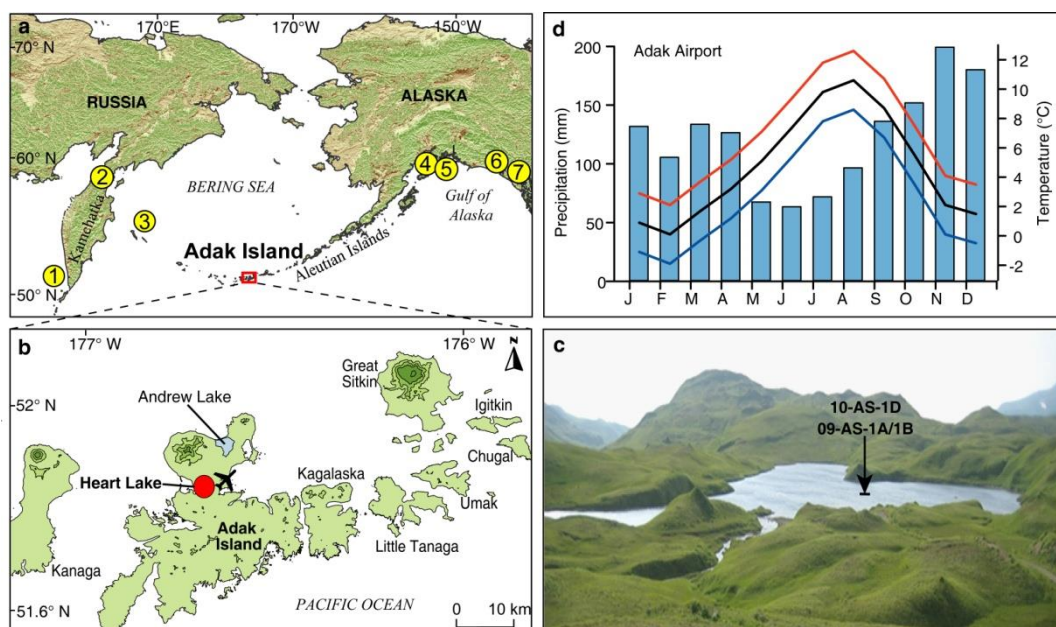
89 To address this, we present the first Holocene oxygen isotope record from the
90 Aleutian Islands in south west Alaska. Our isotope measurements derive from siliceous
91 diatoms ($\delta^{18}\text{O}_{\text{diatom}}$) preserved in the sediments of Heart Lake, on Adak Island (Fig. 1b), and
92 are supported by diatom assemblage analysis of the same sedimentary sequence. We build on
93 earlier work by Bailey *et al.* [2015] who demonstrate that Heart Lake $\delta^{18}\text{O}_{\text{diatom}}$ values
94 correlate significantly with North Pacific climate indices over the past hundred years ($r =$
95 0.43 ; $p < 0.02$, $n = 28$). Here, we apply this empirically-derived understanding to interpret
96 new $\delta^{18}\text{O}_{\text{diatom}}$ data from a longer Heart Lake sediment core which extends back to 9.6 ka.
97 The primary aims are to: (1) investigate the forcing and response of this remote region to a
98 warming climate system as it transitioned from the last glacial period; (2) develop a Holocene
99 reconstruction of North Pacific atmospheric circulation; and (3) bridge the gap in the regional
100 network of proxy records to synthesise and assess spatio-temporal patterns of natural climate
101 variability across Beringia.

102

103 **2. Regional Setting**

104 Heart Lake is a small ($\sim 0.25 \text{ km}^2$), freshwater through-flow system on Adak Island in the
105 central North Pacific (51.85° N , 176.69° W) (Fig.1c). The island is volcanic and forms part

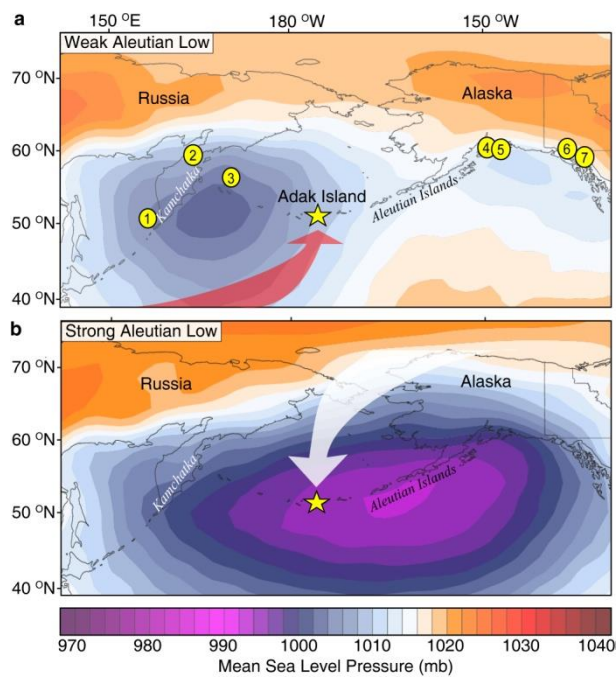
106 of the 1900-km-long Aleutian archipelago extending from mainland Alaska to the Russian-
 107 Kamchatka Peninsula. The lake watershed area is $\sim 8 \text{ km}^2$ and is situated in low-relief hills
 108 surrounded by mountainous terrain (Fig. 1c). There is a single lake basin with a maximum
 109 depth of 8 m. One stream inflows from two larger lakes and a small outflow channel drains to
 110 the Bering Sea $\sim 2 \text{ km}$ to the west. Lake volume is $\sim 8 \times 10^5 \text{ m}^3$ and water retention is an
 111 estimated two weeks, based on the available stream gauge inflow data [TDX, 2013].
 112 Inspection of available satellite imagery reveals that Heart Lake freezes over in winter and
 113 this ice surface remains into spring [USGS, 2017].



114
 115 **Figure 1. Location of (a) Adak Island in the central Aleutian Islands; (b) Heart Lake**
 116 **and Andrew Lake; (c) oblique north west view of Heart Lake with the inflow channel**
 117 **visible in the foreground [credit: Yarrow Axford]; and (d) monthly mean precipitation**
 118 **(blue bars) and surface air temperature at Adak airport (1949–2016), whereby solid**
 119 **lines depict mean (black), minimum (blue) and maximum (red) temperatures [NOAA,**
 120 **2017]. Numbered circles in 1a indicate key sites referred to in text: (1) LV29-114-3 [Max**
 121 **et al. 2012], (2) Pechora Lake [Hammarlund et al. 2015], (3) SO201-12-77KL [Max et al.**
 122 **2012], (4) Horse Trail Fen [Jones et al. 2014], (5) Mica Lake [Schiff et al. 2009], (6)**
 123 **Mount Logan [Fisher et al. 2008], and (7) Jellybean Lake [Anderson et al. 2005]**

124 Adak Island has a mild maritime climate compared to mainland Alaska and is
125 strongly affected by persistent fog and light rain in the summer, and frequent storms and
126 strong winds during winter [Rodionov *et al.* 2007]. Mean annual air temperature is +4.3 °C,
127 and mean winter (December–February) and summer (June–August) values are +1.0 °C and
128 +9.0 °C, respectively (1949–2016) [NOAA, 2017]. Mean December and July precipitation is
129 163 mm and 71 mm, respectively (Fig. 1d) [NOAA, 2017]. Of the total 1.3 m annual
130 precipitation, ~75 % (1.0 m) falls from September to February.

131 The regional climate reflects the configuration of large scale atmospheric–ocean
132 systems, namely the Aleutian Low: a synoptic-scale feature of mean low sea level pressure
133 (SLP) and the leading driver of North Pacific climate [Mock *et al.* 1998]. When the Aleutian
134 Low is ‘weak’, storms tend to track north over the central Aleutian Islands (Fig. 2a); when
135 the pressure system is ‘strong’, storms track south of the Aleutians and into the Gulf of
136 Alaska (Fig. 2b) [Mock *et al.* 1998; Rodionov *et al.* 2007]. These circulation patterns vary on
137 interannual to decadal timescales and induce characteristic climate responses that are well
138 expressed in coupled modes of the North Pacific Index (NPI) and the Pacific Decadal
139 Oscillation (PDO) [Trenberth and Hurrell, 1994; Mantua *et al.* 1997]. Typically, a strong
140 Aleutian Low (–NPI/+PDO) will induce positive sea surface temperatures (SST), surface air
141 temperatures (SAT), and precipitation anomalies in the Gulf of Alaska and negative
142 anomalies in the central North Pacific, with contrary conditions during a weak Aleutian Low
143 (+NPI/–PDO) (see Supplementary Fig.1).



144

145 **Figure 2. Mean winter (December–February) sea level pressure associated with the six**
 146 **most positive (a) and negative (b) North Pacific Index (NPI) values between 1950 and**
 147 **2017 [Trenberth and Hurrell, 2004]. A negative (positive) NPI is a strong (weak)**
 148 **Aleutian Low. Arrows highlight the direction of the primary storm tracks delivering**
 149 **precipitation to our site on Adak Island (yellow star) [Bailey et al. 2015]. SLP data**
 150 **obtained from NCEP/NCAR V1 reanalysis [Kalnay et al. 1996]. Numbered yellow circles**
 151 **in (a) indicate locations of the (1) LV29-114-3 [Max et al. 2012], (2) Pechora Lake**
 152 **[Hammarlund et al. 2015], (3) SO201-12-77KL [Max et al.2012], (4) Horse Trail Fen**
 153 **[Jones et al. 2014], (5) Mica Lake [Schiff et al. 2009], (6) Mount Logan [Fisher et al.**
 154 **2008], and (7) Jellybean Lake [Anderson et al. 2005] climate records discussed in text.**

155

156 3. Materials and Methods

157 3.1. Sediment and water recovery

158 Sediment cores and bottom lake water samples were recovered from Heart Lake during the
 159 summers of 2009 and 2010. A Garmin GPS sonar was used to survey its bathymetry and
 160 reveals that Heart Lake comprises of a single basin with a maximum depth of 8 m,

161 surrounded by a shallow platform < 2 m deep (see Supplementary Figure 2). Coring sites
162 were selected adjacent? (in the vicinity?) of the deepest part of the basin at a depth of 7.6 m.
163 Seven sediment cores were extracted using percussion and hand-held gravity coring devices
164 operated from a floating platform. Bottom lake water samples were collected *in situ* at the
165 sediment-water interface during gravity coring. Following core extraction water was
166 immediately siphoned and sealed in 50 ml vials, ensuring no head space. (why did water
167 sampling have to proceed immediately after core extraction? Were they not sampled using a
168 niskin sampler or similar?) Sediment cores were then split lengthways, packaged, and
169 shipped with water samples to Northern Arizona University where they were stored at 4°C
170 until they were sub-sampled and analyzed. Our study focuses on the longest percussion core
171 (10-AS-1D; 5.9 m) and two accompanying surface gravity cores (09-AS-1A, 0.81 m; and 09-
172 AS-1B, 0.44 m). For a detailed description of the sediment core's lithostratigraphy, see
173 *Krawiec et al.* [2013].

174 **3.2. Chronology**

175 The composite age model for 10-AS-1D and 09-AS-1A is presented in a separate paper
176 devoted to the tephrostratigraphy and radiometric dating of the Heart Lake sedimentary
177 sequence [*Krawiec et al.* 2013]. In summary, a Monte Carlo approach was employed to
178 model the age-depth relation of 16 macrofossil AMS radiocarbon (¹⁴C) dates, together with a
179 peak in recent ²³⁹⁺²⁴⁰Pu activity and the age of the sediment-water interface (2009 AD)
180 [*Krawiec et al.* 2013]. Tephrostratigraphy was used to independently cross check the
181 accuracy of the chronology, whereby the ages of down core tephra horizons from Heart Lake
182 were compared with tephra ages from nearby Andrew Lake and previously published outcrop
183 studies [*Krawiec et al.* 2013]. The chronology for surface core 09-AS-1B derives from
184 radiometric dating of ²¹⁰Pb, ²²⁶Ra, ¹³⁷Cs and ²⁴¹Am by direct gamma assay on 14 dried
185 sediment samples from the upper core section [*Bailey et al.* 2015]. The cores were cross-

186 correlated using a prominent tephra horizon found in all three sedimentary sequences
187 [*Krawiec et al.* 2013; *Bailey et al.* 2015]. All ages herein are expressed as thousands of
188 calendar years (ka) prior to 1950 AD, where 1 ka = 1000 cal yr BP.

189

190 3.3. Stable isotope analyses

191 A total of 147 sediment samples were processed for $\delta^{18}\text{O}_{\text{diatom}}$ analysis. These samples range
192 in age from 9.6 ka (587 cm depth) to 2009 AD, and are sub-/decadally resolved for the most
193 recent 1500 years and at centennial resolution thereafter. From the 5.9 m long core 10-AS-
194 1D, 1 cm³ of sediment (i.e. a 1-cm-thick sample – this doesn't quite make sense – it must
195 have been a very small diameter corer for 1 cm thickness to yield 1 cm³ of sediment?) was
196 extracted at 7 cm intervals from the base (587 cm) to the top of the core. This was the optimal
197 sampling resolution to avoid tephra layers which could potentially cause contamination issues
198 [*Lamb et al.* 2007] – sounds slightly disingenuous as can't imagine that >80% of the core was
199 tephra – why not leave this sentence out? The surface cores 09-AS-1A and 09-AS-1B were
200 both sampled in contiguous 0.5 cm increments. This detail was used to capture sub-decadal
201 changes in $\delta^{18}\text{O}_{\text{diatom}}$ over the past century for direct comparison with instrumental records
202 [see *Bailey et al.* 2015]

203

204 Sediment samples were prepared using a hybrid process of chemical digestion,
205 sieving, and heavy liquid separation adapted from *Morley et al.* [2004]. To remove organic
206 and carbonate material, samples were treated with 30% H₂O₂ at 90°C until reactions ceased,
207 before using 5 % HCl at ambient temperature. Samples were then centrifuged in sodium
208 polytungstate (3Na₂WO₄·9WO₃·H₂O) (SPT) heavy liquid at 2500 rpm for 20 minutes,
209 resulting in the separation and suspension of diatoms from the heavier detritus. This
210 procedure was repeated three times for each sample using specific gravities of 2.50, 2.30 and
211 2.25 g ml⁻¹. After the final SPT separation, samples were washed five times in ultrapure water

212 (UPW) at 1500 rpm for 5 minutes and vacuum filtered through a 3 μm cellulose nitrate
213 membrane to remove potential clay minerals and/or broken diatom fragments. The < 3 μm
214 fraction was discarded as it was too small (< 1 mg) to be analyzed and, upon further
215 inspection (need to put an 'a' in here if keeping this in) contained only small broken diatom
216 fragments and detritus. The remaining samples were treated with a final stage of 30 % H_2O_2
217 at 60 °C for one week to ensure no traces of organic matter remained.

218 Purified diatom samples were analyzed for $\delta^{18}\text{O}_{\text{diatom}}$ using the stepwise fluorination
219 method [Leng and Sloane, 2008] at the NERC Isotope Geosciences Laboratory in Keyworth,
220 UK. The outer hydrous layer of the diatom was removed in a pre-fluorination stage using a
221 BrF_5 reagent at low temperature [Leclerc and Labeyrie, 1987]. This was followed by a full
222 reaction at high temperature to liberate oxygen that was converted to CO_2 [Clayton and
223 Mayeda, 1963] and measured for $\delta^{18}\text{O}_{\text{diatom}}$ using a MAT 253 dual-inlet mass spectrometer.
224 Replicate analyses indicate an analytical reproducibility of ± 0.19 ‰ (1σ) for the samples, and
225 ± 0.30 ‰ (1σ) for the diatom standard BFC_{mod} . All $\delta^{18}\text{O}$ values were converted to the Vienna
226 Standard Mean Ocean Water (VSMOW) scale using the BFC_{mod} standard for calibration.

227 Two Heart Lake water samples were measured for their oxygen and hydrogen (δD)
228 isotope composition using a Thermo-Finnigan Deltaplus XL gas mass spectrometer at the
229 Colorado Plateau Stable Isotope Laboratory, Northern Arizona University, USA. Analytical
230 precision on internal working standards was ± 0.1 ‰ for $\delta^{18}\text{O}$ and ± 1 ‰ for δD . All values are
231 reported here in per mil (‰) relative to VSMOW.

232

233 **3.3.1. Contamination assessment**

234 All purified diatom samples ($n = 147$) were visually inspected for contamination using an
235 OLYMPUS BX40 light microscope. Thirty samples were selected down-core and further
236 inspected using a Hitachi S-4700 field emission scanning electron microscope (SEM). In
237 addition, fourier transform infrared spectroscopy (FTIR) was applied to assess the chemical

238 composition and sample purity of 16 diatom samples from core 10-AS-1D [Swann and
239 Patwardham, 2011]. These samples, together with the BFC_{mod} diatom standard, were
240 analyzed using FTIR at the British Geological Survey in Keyworth, UK [Bailey et al. 2014].
241 FTIR analyses of all purified diatom isotope samples measured indicate peaks corresponding
242 to the BFC_{mod} standard, known to represent clean, fossilised diatomite (Supplementary Fig.
243 3). Spectral deviation from the standard would indicate additional compounds and
244 contamination by non-diatom components [Swann and Patwardhan, 2011]; peaks centred at
245 ~450 cm⁻¹, ~800 cm⁻¹ and ~1100 cm⁻¹ confirm pure silica and the integrity of our diatom
246 isotope samples [Bailey et al. 2014].

247

248 **3.4. Diatom assemblage analysis**

249 Fifty-seven sub-samples of the purified diatom material used for $\delta^{18}\text{O}_{\text{diatom}}$ analysis were
250 retained for diatom species analysis. These include 33 samples selected at c. 13 cm intervals
251 from AS-10-1D, and 24 samples at a contiguous 0.5 cm resolution from AS-09-1B. Diatom
252 slides were prepared on a hot plate using Naphrax[®] mounting medium. A minimum of 300
253 diatom frustules per sample were counted along transects at x1000 magnification, under an
254 OLYMPUS BX40 light microscope. Taxonomic identification was based on classifications in
255 *Camburn and Charles* [2000] and *Krammer and Lange-Bertalot* [1986–1991].

256 Following diatom identification, species counts were converted to percentage
257 abundance and evaluated using the software package Tilia (v.2.0.41) [Grimm, 2015]. For
258 diatom zone demarcation, a constrained incremental sum-of-squares cluster analysis
259 (CONISS) [Grimm, 1987] was applied to all dominant taxa with a relative abundance >5 %
260 in at least one sample. To quantitatively assess [down core trends in diatom assemblages](#), a
261 principal components analysis (PCA) [ter Braak and Prentice, 1988] was applied to a
262 correlation matrix based on the dominant (>5 %) diatom species in all 57 samples. The

263 analysis was performed on untransformed percentage data using the program C2 (v.1.7.6)
264 [Juggins, 2014].

265

266 **4. Results**

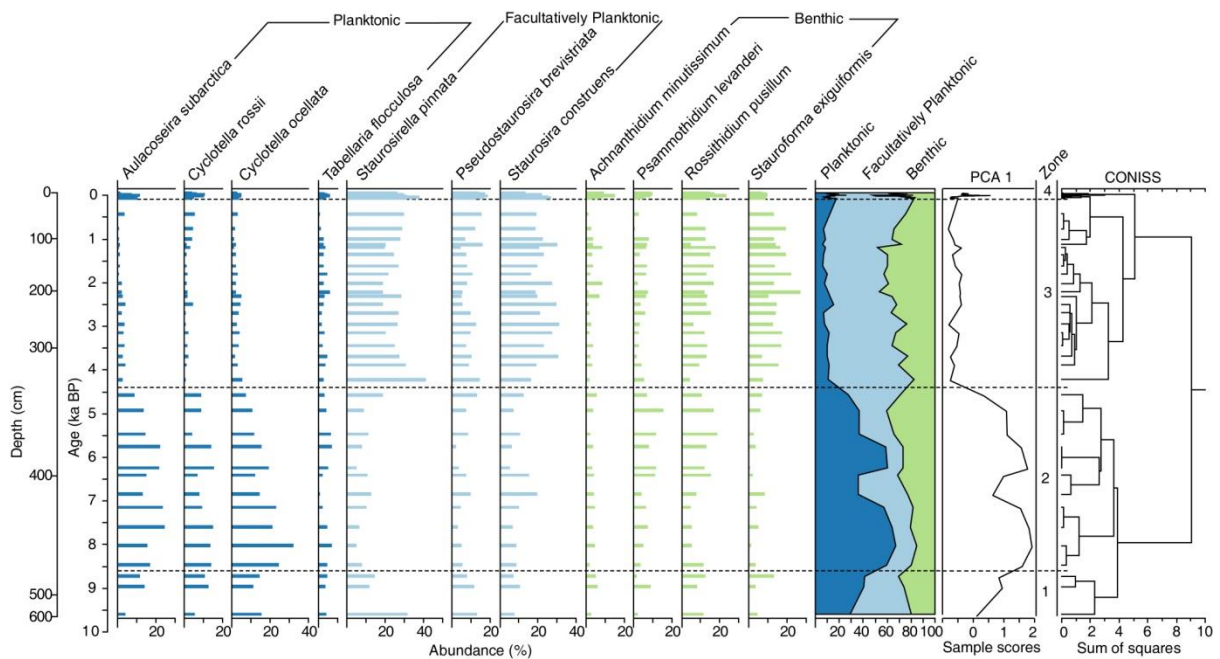
267 **4.1. Diatom flora**

268 Diatom frustules are well preserved in all samples and show no sign of valve dissolution. The
269 flora is diverse and a total of 155 different freshwater diatom species were identified. Of
270 these, 11 species account for > 90 % of all diatoms present in all samples. These include
271 species belonging to the genera *Aulacoseira*, *Cyclotella*, *Rossethidium*, and small fragilarioid
272 taxa (consisting of the genera *Fragilaria*, *Pseudostaurosira*, *Staurosira*, *Stauroforma*, and
273 *Staurosirella*). Species with an abundance ≥ 5 % in at least one stratigraphic level are
274 presented (Fig. 3), and the record is divided into four zones based on the CONISS
275 dendrogram: *Zone 1* (9.6–8.6 ka; 587–452 cm), *Zone 2* (8.6–4.4 ka; 452–352 cm), *Zone 3*
276 (4.4 ka–1860 AD; 352–13.25 cm), and *Zone 4* (1860–2009 AD; 13.25–0 cm). Species are
277 grouped into one of three habitat types (planktonic, benthic, or facultatively planktonic) based
278 on classifications by Spaulding *et al.* [2017] (Fig. 3).

279 Diatom *Zone 1* (587–452 cm; ca. 9.6–8.6 ka) is dominated by *Staurosirella pinnata*
280 (33 %), *Cyclotella ocellata* (18 %), and other small fragilarioid taxa (60 %) (Fig. 3). By ca.
281 9.0 ka the abundance of *S. pinnata* decreases to 10 % and the planktonic species *Cyclotella*
282 *rossii* (10–30 %), *Aulacoseira subarctica* (4–25 %) and *Cyclotella ocellata* (5–14 %) are
283 more dominant. Some of the small benthic species all show slight increases in abundance at
284 this time, including *Psammothidium levanderi* (9 %) and *Achnantheidium minutissimum* (6%),
285 albeit at a low relative abundance.

286 In *Zone 2* (452–352 cm; ca. 8.6–4.4 ka) the planktonic species *C. ocellata*, *A.*
287 *subarctica*, and *C. rossii* begin to dominate the assemblage (Fig. 3). Collectively these
288 species reach a maximum abundance of 75 % between 8.5–7.6 ka; a time when small benthic

289 and facultatively planktonic taxa are at their overall lowest Holocene abundances (0–5 %).
 290 Increases in abundances of *Rossithidium pusillum* and other small fragilarioid taxa occur *ca.*
 291 7.6 and 6.8 ka, concurrent with a decrease in planktonic taxa (Fig. 3). After *ca.* 5.0 ka, the
 292 abundance of planktonic species gradually decrease, paralleled by increasing abundance of
 293 facultatively planktonic taxa.
 294



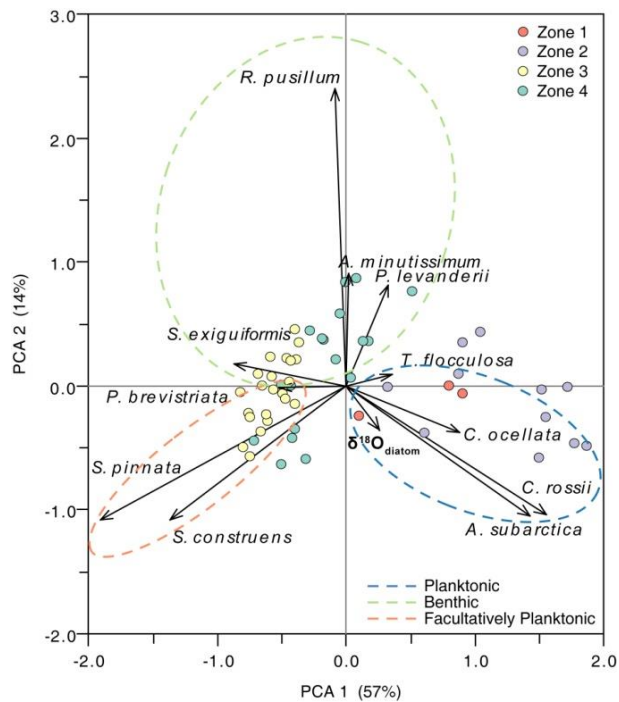
295
 296 **Figure 3. Heart Lake diatom stratigraphy and Principal Components Analysis (PCA)**
 297 **scores of the 11 dominant diatom species (>5 % abundance), grouped by habitat**
 298 **preference. Diatom zone demarcation (dashed lines 1–4) is guided by the CONISS**
 299 **cluster analysis. Variables are plotted on a linear timescale (ka BP) and the depth scale**
 300 **refers to depth below lake floor.**

301
 302 At the onset of Zone 3 (352–13.25 cm; 4.4 ka–1860 AD) a large increase in the
 303 facultatively planktonic taxa is paralleled by declines in planktonic taxa (Fig. 3). Collectively,
 304 the small fragilarioid taxa make up ~80 % of the assemblages in this zone and several species
 305 attain their maximum Holocene abundance, including *S. pinnata* at 4.2 ka (39 %) and
 306 *Staurosira construens* at 3.8 ka (28 %). In contrast, planktonic species decline from a mean

307 abundance of 55 % in Zone 2, to 5 % in Zone 3. Only *Tabellaria flocculosa* shows relatively
308 little change in abundance from Zone 2, remaining at ~4%. Of the benthic taxa, *Stauroforma*
309 *exiguiformis* and *R. pusillum* are also present in high abundances throughout Zone 3, with the
310 former attaining a maximum Holocene abundance of 26 % at *ca.* 2.2 ka.

311 In Zone 4 (13.25–0 cm; *ca.* 1860–2009 AD) the small fragilarioid taxa continue to
312 dominate the assemblage, comprising ~75 % of the total assemblage *ca.* 1910 AD (Fig. 3).
313 After this time, the abundance of facultatively planktonic taxa steadily decreases as the
314 benthic and planktonic species increase. After *ca.* 1970 AD, the numbers of *A. subarctica*
315 decreases substantially, such that only a few individual frustules were counted per sample.

316 Stratigraphic changes in diatom flora are captured in the first two PCA components,
317 which collectively account for 71 % of the total assemblage variance (Fig. 4). Additional
318 eigenvectors defined by the PCA (3–5) were not considered given they explain progressively
319 lower proportions of the total variance ($\lambda_3=0.108$, $\lambda_4=0.059$, $\lambda_5=0.038$). PCA 1 represents 57
320 % of total variance and correlates to the planktonic species at the positive extreme, and the
321 facultatively planktonic species at the negative extreme. PCA 2 accounts for 14 % of total
322 variance, and correlates to the small fragilarioid taxa (Fig. 4). The Holocene succession of
323 diatom communities in Heart Lake is further illustrated by the time-series of the 54 sample
324 scores on PCA axis 1 (Fig. 3).



325

326

327

328

329

330

331 4.2. Oxygen isotopes

332

333

334

335

336

337

338

339

340

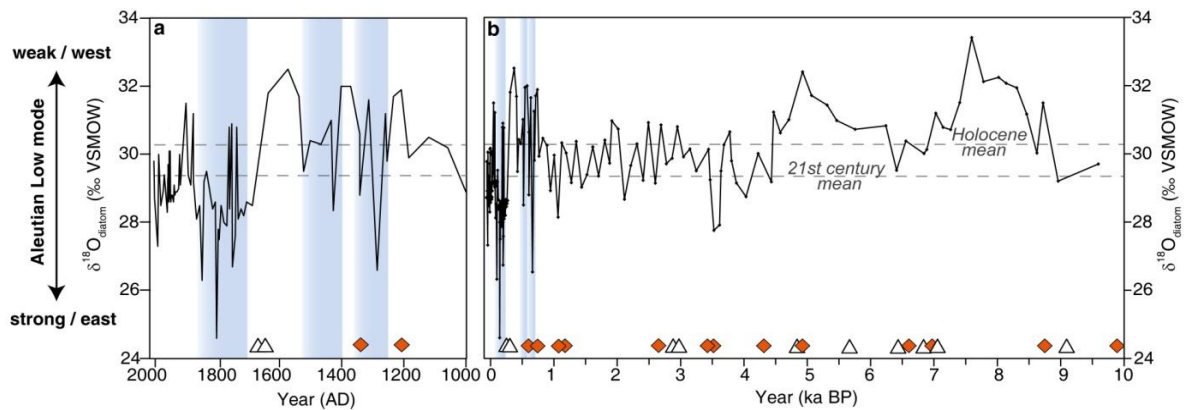
341

Figure 4. Loadings of the 11 dominant diatom taxa from Heart Lake and their corresponding PCA scores. Sample scores (circles) are coloured according to their down core diatom assemblage Zone (1–4). Dashed coloured ellipses group diatom species by their habitat preference.

Holocene $\delta^{18}\text{O}_{\text{diatom}}$ values vary between 24.6 ‰ (1805 AD) and 33.3 ‰ (7.6 ka) ($\bar{x} = 29.7$ ‰, $n = 137$) (Fig. 5) with a range of ± 8.7 ‰ that is appreciably greater than the standard deviation of all samples (± 0.19 ‰) and diatom standards (± 0.30 ‰) measured. The base of the Heart Lake sediment core has a $\delta^{18}\text{O}_{\text{diatom}}$ value of 29.7 ‰ at 9.6 ka, and values steadily increase to the maximum Holocene value of 33.3 ‰ at *ca.* 7.6 ka (Fig. 5). After 4.9 ka $\delta^{18}\text{O}_{\text{diatom}}$ becomes progressively lower until *ca.* 3.5 ka (27.8 ‰) where values remain stable at ~ 29 –30 ‰ until *ca.* 1.0 ka. After *ca.* 1.0 ka, $\delta^{18}\text{O}_{\text{diatom}}$ exhibits high variability to lower values *ca.* 1250–1340 AD and 1430–1525 AD, and after 1640 AD there is a shift to overall lower $\delta^{18}\text{O}_{\text{diatom}}$ values, including the Holocene minimum $\delta^{18}\text{O}_{\text{diatom}}$ value of 24.6 ‰ at 1805 AD. The $\delta^{18}\text{O}_{\text{diatom}}$ values then slightly increase between 1805–1903 AD, before decreasing

342 to the present day (29.8 ‰) (Fig. 5). Using the sub-division age of 4.2 ka for the mid-late
343 Holocene boundary [Walker et al. 2012], late Holocene $\delta^{18}\text{O}_{\text{diatom}}$ is significantly ($p < 0.001$)
344 lower than in the early–mid Holocene.

345



346

347 **Figure 5. Time series of Heart Lake $\delta^{18}\text{O}_{\text{diatom}}$ during (a) the past millennium and (b) the**
348 **Holocene. Horizontal dashed grey lines indicate the Holocene and the 21st century**
349 **$\delta^{18}\text{O}_{\text{diatom}}$ value. Orange diamonds and white triangles indicate previously published**
350 **radiocarbon ages and tephra beds, respectively [Krawiec et al. 2013]. Vertical blue bars**
351 **correspond to three intervals of Little Ice Age glacier advance in mainland Alaska**
352 **[Solomina et al. 2015].**

353 5. Discussion

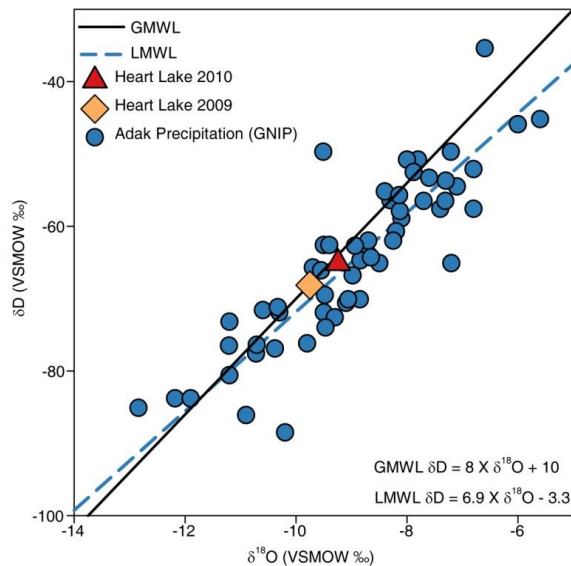
354 5.1. Oxygen isotope paleohydrology and paleoclimatology

355 Oxygen isotope ratios measured in precipitation ($\delta^{18}\text{O}_{\text{P}}$) at Adak airport (1962–67, 1972–73;
356 $n = 60$) indicate mean annual precipitation-weighted $\delta^{18}\text{O}_{\text{P}}$ is -8.8 ‰, with small seasonal
357 differences between January (-9.4 ‰) and July (-8.9 ‰) [IAEA/WMO, 2017]. The
358 correspondence between Heart Lake water $\delta^{18}\text{O}$ and the local and global meteoric water lines
359 confirms that (1) Heart Lake water $\delta^{18}\text{O}$ reflects local precipitation, and (2) evaporative
360 effects influencing precipitation and lake water $\delta^{18}\text{O}$ are minimal with no isotopic enrichment
361 (Fig. 6). Specifically, the two Heart Lake bottom water ($\delta^{18}\text{O}_{\text{water}}$) samples collected in

362 summer 2009 and 2010 ($\bar{x} = -9.5 \text{ ‰}$) are directly comparable, within error, to the long term
363 winter and spring $\delta^{18}\text{O}_\text{P}$ values from Adak airport. These data indicate the lake water budget
364 is dominated by winter and spring precipitation (i.e. snowfall and melt) similar to many lakes
365 and streams across Alaska [Clegg and Hu, 2010; Lachniet et al. 2016; Vachula et al. 2017].

366 There is no correlation between mean monthly $\delta^{18}\text{O}_\text{P}$ and SAT ($r = 0.15$, $n = 72$) or
367 precipitation amount ($r = 0.03$, $n = 72$) at Adak airport. Instead, Bailey et al. [2015] found
368 that Adak Island $\delta^{18}\text{O}_\text{P}$ values are primarily controlled by the moisture source and trajectory
369 of local precipitating storm systems. Specifically, winters with intensified Aleutian Low
370 circulation are characterized by precipitation with significantly ($p < 0.05$) lower than mean
371 $\delta^{18}\text{O}_\text{P}$ values. These variations are explained by systematic shifts in the central foci of the
372 Aleutian Low; when the SLP minimum is near Adak (strong Aleutian Low), polar air masses
373 are drawn south and advect water vapor and precipitation that is relatively depleted in ^{18}O ,
374 along with lower-than-average winter temperatures and increased snowfall (Fig. 2b)
375 [Rodionov et al. 2007; Bailey et al. 2015]. In contrast, a weakened and westerly displaced
376 Aleutian Low increases the southerly Pacific moisture flux to Adak via an enhanced south-
377 westerly storm track (Fig. 2a) [Rodionov et al. 2007]. These systems carry warm ^{18}O -
378 enriched moisture, and bring higher-than-average temperatures and increased precipitation to
379 Adak Island [Bailey et al. 2015].

380



381

382

383

384

385

386

387

388

389

390

391

392

393

394

395

396

397

398

399

Figure 6. Heart Lake surface water $\delta^{18}O$ (2009 and 2010) on the local meteoric water line (LMWL) and the global meteoric water line (GMWL). LMWL data are derived from Adak monthly composite precipitation samples collected by the Global Network of Isotopes in Precipitation (GNIP) [IAEA/WMO, 2017]

$\delta^{18}O_{\text{diatom}}$ is controlled by several environmental parameters which depend on local hydrology, climate, and the seasonality of diatom growth [Barker *et al.* 2001; Rioual *et al.* 2001; Jones *et al.* 2004; Rosqvist *et al.* 2004; Leng and Barker, 2006; Schiff *et al.* 2009; Mackay *et al.* 2011; Meyer *et al.* 2014; Chaplignin *et al.* 2016]. Previous work by Bailey *et al.* [2015] showed that the surface core $\delta^{18}O_{\text{diatom}}$ record from Heart Lake correlates significantly with the winter NPI during the instrumental period (1900–2009 AD) ($r = 0.43$, $p < 0.02$, $n = 28$). This positive relationship confirms that Heart Lake diatoms precipitate their silica frustule in isotopic equilibrium with the lake water in which they grow [Labeyrie, 1974; Leclerc and Labeyrie, 1987], independent of size or species-related vital effects [Bailey *et al.* 2014]. During the spring thaw, it is evident that winter season precipitation ($\delta^{18}O_P$) enters Heart Lake coincident with onset of the spring diatom bloom. A limited component of residual summer growth might be expected, but bulk $\delta^{18}O_{\text{diatom}}$ analysis is weighted toward the main period of diatom growth in spring [Leng *et al.* 2001; Bailey *et al.* 2014]. Under the

400 assumption that similar climatic controls on $\delta^{18}\text{O}_\text{P}$ prevailed before 1900 AD, we use this
401 extended $\delta^{18}\text{O}_{\text{diatom}}$ record as a proxy for atmospheric circulation throughout the Holocene.

402

403 **5.2. Holocene environmental history of Adak Island**

404 **5.2.1. Early-mid Holocene, 9.6 – 4.4 ka**

405 Adak Island, along with the Aleutian chain, was glaciated during the last glacial maximum,
406 though there are few chronological constraints on the onset and pattern of ice retreat [Coats,
407 1956; Bradley, 1948; Fraser and Snyder, 1959; Black, 1976]. At Heart Lake, percussion
408 coring ceased at a depth of 587 cm without penetrating bedrock or till, indicating the
409 catchment deglaciated prior to 9.6 ka.

410 From 9.6–9.0 ka, the dominance of fragilarioid and other small benthic taxa reflect a
411 temperate oligotrophic shallow lake with an extensive littoral zone. These pioneering taxa
412 dominate polar to subpolar and mountainous tundra lakes [Lotter and Bigler, 2000; Rühland
413 *et al.* 2003; Hausmann and Pienitz, 2009; Devlin and Finkelstein, 2011] and their presence
414 suggests a relatively short growth season with cool air temperatures [Smol *et al.* 2005;
415 Rühland *et al.* 2008; Hausmann and Pienitz, 2009]. Cool/dry conditions at this time are
416 further supported by low concentrations of biogenic silica (BSi) and organic matter (OM) in
417 nearby Andrew Lake [Krawiec and Kaufman, 2014] and the dominance of *Salix* and
418 *Empetrum* in northern Adak [Heusser, 1978].

419 Heart Lake was increasingly colonized by planktonic diatoms between 9.3–4.4 ka
420 (Fig. 3). Of these, *A. subarctica* is common across Arctic and subarctic zones, and typically
421 shows pronounced periodicity with the spring maximum in non-stratified lakes [Bradbury *et*
422 *al.* 2002; Baier *et al.* 2004; Rioual *et al.* 2007; Gibson *et al.* 2003; Solovieva *et al.* 2015]. It is
423 a heavily silicified species, forming colonies that require turbulence-induced suspension to
424 remain within the photic zone [Rühland *et al.* 2008; Lotter *et al.* 2010], and indicates

425 persistent strong seasonal winds, together with associated turbulent water mixing and nutrient
426 upwelling [Wang *et al.* 2008; Andrén *et al.* 2015; Solovieva *et al.* 2015]. In contrast,
427 *Cyclotella* species have a competitive advantage over the heavily silicified *A. subarctica*
428 during strong stratification [Andrén *et al.* 2015] and typically bloom after ice-out in subarctic
429 regions [Rühland *et al.* 2008; Hoff *et al.* 2015]. In Kamchatka, *Cyclotella* spp. prosper during
430 warmer years [Lepskaya *et al.* 2010], and are broadly considered warm water indicators due
431 to their recent expansion across Arctic lakes [Smol *et al.* 2005; Rühland *et al.* 2008].
432 Collectively, these early-mid Holocene diatom assemblages reveal a phase of overall high
433 lake mixing and turbidity, reduced lake ice cover, and relatively high Si/P ratios [Interlandi *et*
434 *al.* 1999; Rühland *et al.* 2003; Rioual *et al.* 2007]. These changes are further summarized by
435 the Holocene time series of PCA 1 sample scores (Fig. 3).

436 The isotope composition of Heart Lake water was significantly ($p < 0.001$) higher
437 during the early-mid Holocene compared to the late Holocene (Fig. 5), reflecting the
438 prevalence of southerly storms delivering abundant precipitation with higher $\delta^{18}\text{O}$ values
439 [Bailey *et al.* 2015]. Such warm, southerly winter storms would promote turbulent mixing
440 and limit the development of winter lake ice, thereby extending the open-water growing
441 season and allowing for a spring diatom assemblage dominated by planktonic species (Fig.
442 3). *Aulacoseira subarctica*, in particular, is abundant in modern lake systems during years
443 with short, warm winters [Gibson *et al.* 2003; Horn *et al.* 2011]. Elevated pollen percentages
444 of *Cyperaceae* and other wetland species in northern Adak also imply warm/wet conditions at
445 this time [Heusser, 1978] and correspond to higher local lake levels prior to 4.0 ka [Krawiec
446 and Kaufman, 2014]. Peak $\delta^{18}\text{O}_{\text{diatom}}$ (33.3 ‰) suggests maximum Holocene warmth at 7.6
447 ka, an inference supported by the simultaneous maximum Holocene abundance of the warm
448 water indicator *C. ocellata* [Rühland *et al.* 2008] (Fig. 3).

449 The $\delta^{18}\text{O}_{\text{diatom}}$ record correlates positively with the time series of PCA 1 scores ($r =$
450 0.48, $p < 0.001$) and demonstrates that diatom community structure is indirectly connected to

451 climate over millennial timescales. It also indicates that diatom species changes are a natural
452 ecological response to climatically-driven shifts in lake water $\delta^{18}\text{O}$, as reflected in the
453 $\delta^{18}\text{O}_{\text{diatom}}$ record, rather than the converse (i.e. changes in diatom species drive $\delta^{18}\text{O}_{\text{diatom}}$
454 variation).

455

456 **5.2.2. Mid-late Holocene, 4.4 ka – present**

457 At around 4.4 ka, a major shift in diatom composition occurred with marked changes from a
458 predominantly planktonic assemblage to the dominance of small fragilarioid and benthic taxa
459 (Fig. 3). During this transition the relatively warm, deep, and well-mixed open-water
460 conditions of the early-mid Holocene (9.6–4.4 ka) gave way to a less turbulent, potentially
461 shallower lake. This transition coincides with a shift to lower $\delta^{18}\text{O}_{\text{diatom}}$ values in the late
462 Holocene, reflecting an increase of isotopically depleted water (i.e. snow and/or ice melt)
463 during the spring thaw [Bailey *et al.*, 2015; Streletskiy *et al.* 2015], and reduced warm, ^{18}O -
464 enriched southerly storms that characterized the early-mid Holocene.

465 An increase in northerly winds and lower temperatures during the late Holocene
466 would have enhanced formation of winter lake ice, which in turn was insulated and prolonged
467 by increased winter snowfall [Mock *et al.* 1998]. Persistence of lake ice into the spring
468 shortens the aquatic growth season and restricts light penetration into the water column
469 during the spring bloom, thereby precluding the growth and development of planktonic
470 communities requiring an ice-free lake for photosynthesis and a turbulent, well-mixed water
471 column. Instead, the mid-late Holocene flora at Heart Lake is dominated by fragilarioid
472 species known to colonise benthic and periphytic habitats under lake ice cover [Lotter and
473 Bigler, 2000; Douglas and Smol, 2010; Biskaborn *et al.* 2016]. These benthic communities
474 would have further benefitted from the absence of competition for nutrients from planktonic
475 diatoms, which do not thrive under ice [Lepskaya *et al.* 2010; Roberts *et al.* 2015]. A
476 reduction in turbulent wind-driven lake mixing at this time may have also been responsible

477 for increased benthic production and a simultaneous expansion of the littoral zone and
478 benthic habitat [Bradbury, 1988]. Increased winter precipitation and subsequent spring snow
479 melt would account for the sedimentation increase at 3.8 ka from 0.2 to 0.8 mm/yr [Krawiec
480 and Kaufman, 2014]. This turbidity would have further reduced light penetration into the
481 benthic zone, thereby promoting fragilarioid taxa which thrive under limited light and
482 generally turbid conditions [Lotter and Bigler, 2000; Douglas and Smol, 2010].

483 The simultaneous changes in diatom species assemblages and $\delta^{18}\text{O}_{\text{diatom}}$ values *ca.* 4.4
484 ka reflect numerous factors affecting vertical mixing patterns, availability of resources (e.g.
485 light, nutrients), and thereby the algal production and composition of Heart Lake. These
486 pronounced changes broadly coincided with other paleoenvironmental changes on Adak
487 Island centred *ca.* 4.4 ka. For example the BSi and inferred chlorophyll-*a* record from nearby
488 Andrew Lake also indicates increased aridity after 4.0 ka [Krawiec and Kaufman, 2014],
489 while reconstructed plant assemblages show a reduction in *Cyperaceae* after *ca.* 4.5 ka as
490 cooler/drier conditions prevailed over Adak Island [Heusser, 1978].

491 Between 950 AD and 1200 AD, higher $\delta^{18}\text{O}_{\text{diatom}}$ indicates a transition to overall
492 warmer and wetter conditions on Adak (Fig. 5). A decrease in *Empetrum* vegetation across
493 northern Adak also indicates increased moisture [Heusser, 1978], while Krawiec and
494 Kaufman [2014] interpret sustained low BSi and chlorophyll-*a* content from Andrew Lake as
495 the stormiest interval on record. Our $\delta^{18}\text{O}_{\text{diatom}}$ values exhibit high variability between 950
496 and 1900 AD, implying the local climate was also wetter and more variable since 950 AD.
497 These conditions would account for the continued dominance of fragilarioid taxa over this
498 period with unstable lake conditions [Smol *et al.* 2005; Rühland *et al.* 2008; Hausmann and
499 Pienitz, 2009]. Additionally, a peak in sedimentation *ca.* 1.0 ka, attributed to increased
500 storminess [Krawiec and Kaufman, 2014], rendered conditions unfavourable for planktonic
501 diatom species due to increased sediment suspension and reduced light penetration. Unlike
502 numerous diatom assemblage records across the subarctic and Arctic, in Heart Lake there is

503 no major shift toward those taxa favouring longer growing seasons under warming climatic
504 conditions (e.g. *Cyclotella*) [Smol *et al.* 2005]. Conversely, benthic assemblages show an
505 increase after *ca.* 1860 AD (Fig. 3), reflecting an overall strengthening of Aleutian Low
506 circulation since 1900 AD [Trenberth and Hurrell, 1994] and increasingly unstable
507 environmental conditions on Adak Island over the past century. These findings are consistent
508 with observations in North America and Greenland that suggest shifts in *Cyclotella*
509 abundances are more closely related to lake mixing, water clarity and resource availability,
510 rather than direct temperature effects [Saros and Anderson, 2015].

511

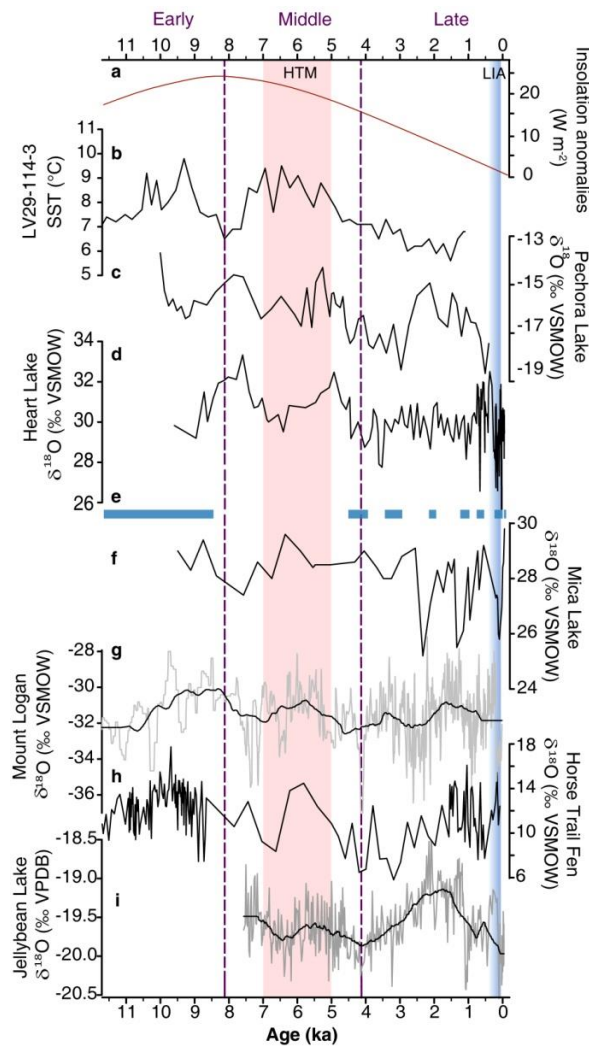
512 **5.3. Regional paleoenvironmental context**

513 Our $\delta^{18}\text{O}_{\text{diatom}}$ reconstruction reveals distinct shifts in the prevailing trajectory of storm
514 systems delivering moisture to Adak Island. The primary trends suggest a relatively weak and
515 westerly positioned Aleutian Low during the early-mid Holocene (9.7–4.5 ka), with a
516 strengthening eastward shift after *ca.* 4.5 ka (Fig. 5). Based on 21st century observations,
517 typical climatic responses to a weakened Aleutian Low are: (1) a weakening of Pacific mid-
518 latitude storm tracks; (2) increased meridional flow to the central-western Bering Sea; and (3)
519 reduced winter sea surface heat loss in the central-western Bering Sea and enhanced heat loss
520 from the Okhotsk Sea [Mock *et al.* 1998; Rodionov *et al.* 2007]. Under this synoptic regime
521 the following conditions would be anticipated in regional paleoclimate records: (1) a
522 reduction in winter storms and precipitation in the Gulf of Alaska region; (2) positive
523 precipitation and temperature anomalies in the central-western Aleutian Islands; and (3) SST
524 warming and reduced winter sea ice extent in the central-western Bering Sea and contrary
525 conditions in the Okhotsk Sea.

526 In support of this synoptic-scale picture, vegetation and lake-level reconstructions
527 provide independent evidence for considerably drier winter conditions in eastern Beringia
528 during the early-mid Holocene [Anderson *et al.* 2005; RS Anderson *et al.*, 2006; Zander *et al.*

529 2013]. For example, numerous lakes in southern Alaska and the Yukon record lower-than-
530 present water levels during the early Holocene until *ca.* 8 ka [*Kaufman et al.* 2016], reflecting
531 a combination of higher summer temperatures and lower winter precipitation. Furthermore,
532 an inferred decrease in frequency and intensity of winter storms steered into the Gulf of
533 Alaska accounts for marked episodes of glacial retreat at this time [*Solomina et al.* 2015],
534 driven by reduced winter snowfall/accumulation and negative net mass balance.

535 The SST patterns associated with a weakened wintertime Aleutian Low are also
536 evident during the early-mid Holocene. Relatively warm early Holocene SSTs are
537 documented from the western Bering Sea [*Max et al.* 2012], reflecting a persistently negative
538 phase of the PDO during the early-mid Holocene and an increase in Pacific storms tracking
539 into the region [*Rodionov et al.* 2007]. In the Okhotsk Sea, alkenone-derived SST estimates
540 correspond well with Heart Lake $\delta^{18}\text{O}_{\text{diatom}}$ between *ca.* 9.6–5.0 ka (Fig. 7), whereby higher
541 $\delta^{18}\text{O}_{\text{diatom}}$ and an inferred weak Aleutian Low corresponds to lower early-mid Holocene SSTs
542 [*Max et al.* 2012]. This relationship conforms to modern northerly geostrophic wind
543 anomalies during a weakened and westward displaced Aleutian Low that cool and enhance
544 polynya growth in the Okhotsk Sea [*Itaki and Ikahara, 2004; Harada et al.* 2014].
545 Specifically, warm (cold) winter SSTs in the Bering Sea (Okhotsk Sea) presently occur when
546 the Aleutian Low is shifted west and the Siberian High dominates over central western
547 Siberia [*Rodionov et al.* 2007]. These anti-correlated trends also manifest in sea-ice anomalies
548 on weekly to monthly time-scales during the 21st century [*Cavalieri and Parkinson, 1987*]
549 and are linked to the east–west migration of the Siberian High and Aleutian Low.



550

551 **Figure 7. Holocene time series of (a) summer (JJA) insolation at 65°N [Berger and**
 552 **Loutre, 1991], (b) alkenone SSTs from LV29-114-3 in the Okhotsk Sea [Max et al. 2012],**
 553 **(c) Pechora Lake $\delta^{18}\text{O}$ [Hammarlund et al. 2015], (d) Heart Lake $\delta^{18}\text{O}_{\text{diatom}}$ (this record),**
 554 **(e) intervals of expanded mountain glaciers in eastern Beringia [Solomina et al. 2015],**
 555 **(f) Mica Lake $\delta^{18}\text{O}$ [Schiff et al. 2009], (g) Mount Logan ice $\delta^{18}\text{O}$ [Fisher et al. 2008], (h)**
 556 **Horse Trail Fen $\delta^{18}\text{O}$ [Jones et al. 2014], and (i) Jellybean Lake $\delta^{18}\text{O}$ [Anderson et al.**
 557 **2005]. Black lines in (g) and (i) represent 40-yr smoothed intervals. Vertical red shading**
 558 **indicates the eastern Beringia mid-Holocene Thermal Maximum [Kaufman et al. 2016],**
 559 **blue shading indicates the Little Ice Age (LIA) [Solomina et al. 2015].**

560 We find independent support for the Holocene migration of the Siberian High from
561 the Pechora Lake $\delta^{18}\text{O}$ record in northern Kamchatka [*Hammarlund et al.* 2015] (Fig. 7). A
562 north-eastward shift of the Siberian High, concurrent with a strong and eastward shifted
563 Aleutian Low, is linked to periods of increased winter snow contributions to Pechora Lake
564 and overall lower $\delta^{18}\text{O}$ values [*Hammarlund et al.* 2015]. The coherency of abrupt and
565 persistent change between the Heart and Pechora Lake $\delta^{18}\text{O}$ records between 9.6–3.5 ka
566 provides convincing evidence that the Aleutian Low–Siberian High system prevailed
567 throughout the early-mid Holocene (Fig. 7). Moreover, we propose that the synchronous
568 west-east migration of these systems may have been partially responsible for the non-linear
569 and heterogeneous climatic patterns reconstructed across east and west Beringia at this time
570 [*Brooks et al.* 2015; *Kaufman et al.* 2016].

571 Maximum values of $\delta^{18}\text{O}_{\text{diatom}}$ in Heart Lake at 7.6 ka broadly coincide with the
572 northern high-latitude (65 °N) summer insolation maxima *ca.* 8.0 ka (Fig. 7) [*Berger and*
573 *Loutre* 1991]. Significantly ($p < 0.001$) higher $\delta^{18}\text{O}_{\text{diatom}}$ in Heart Lake – relative to both the
574 modern (1900 AD–present) and long-term (9.6 ka–present) mean $\delta^{18}\text{O}_{\text{diatom}}$ – implies a HTM
575 in the central Aleutian Islands at 7.6 ka characterized by persistently weak Aleutian Low
576 circulation, and coincident with maximum abundances of warm water indicator species [*Smol*
577 *et al.* 2005] (Fig. 3). Similarly, a Holocene SST maximum is evident *ca.* 7.5 ka in both the
578 northwest Pacific [*Minoshima et al.* 2007] and the subarctic North Pacific [*Harada et al.*
579 2014], and from GCMs which indicate maximum SATs and SSTs in the Bering Sea and
580 Aleutian Islands *ca.* 7.0–8.0 ka [*Renssen et al.* 2012]. In southern Kamchatka, the majority of
581 paleoenvironmental records demonstrate a HTM *ca.* 7.0–5.3 ka [*Brooks et al.* 2015],
582 consistent with warm temperatures across eastern Beringia [*Kaufman et al.* 2016]. These
583 results contrast with previous paleoclimate studies from Alaska and the northwest Pacific that
584 identify an earlier HTM at *ca.* 11.3–9.1 ka [*Kaufman et al.* 2004; *Max et al.* 2012]. Such
585 uncertainty in these early Holocene warming patterns is highlighted by *Zhang et al.* [2017]

586 who found large discrepancies between modelled and reconstructed Holocene temperatures
587 across Alaska. Hence, it is difficult to fully constrain the timing of the HTM in the central
588 Aleutian Islands, particularly given that our record does not extend the full Holocene epoch
589 coupled with a paucity of local alternative studies.

590 Simultaneous shifts in diatom flora and $\delta^{18}\text{O}_{\text{diatom}}$ after the HTM at *ca.* 4.5 ka indicate
591 multiple and inter-related environmental changes that impacted Heart Lake. These
592 pronounced changes coincide with local proxy inferences demonstrating increased aridity
593 under a prevailing northerly circulation pattern [*Heusser, 1978; Corbett et al. 2010; Krawiec*
594 *and Kaufman, 2014*]. This mid-Holocene perturbation coincides with a return to cooler
595 conditions, increased winter precipitation and extensive glacial advance in Kamchatka
596 [*Nazarova et al. 2013; Barr and Solomina, 2014; Meyer et al. 2015*]. Widespread cooling is
597 also evident in eastern Beringia during the late Holocene [*Kaufman et al. 2016*], and
598 mountain glaciers across Alaska advanced between *ca.* 4.5 and 3.0 ka [*Solomina et al. 2015*],
599 in phase with those in Kamchatka and demarking onset of the Neoglacial across Beringia
600 [*Savoskul, 1999; Barr and Solomina, 2014*]. Though temperature is proposed as the principal
601 control on regional glacier mass balance through the Holocene [*Solomina et al. 2015*], the
602 observed glacial maxima in Alaska are asynchronous with the timing of pronounced cold
603 intervals [*Kaufman et al. 2016*]. Instead, our data suggest the transition to intensified Aleutian
604 Low circulation after 4.5 ka, coincident with declining summer insolation [*Berger and*
605 *Loutre, 1991*], drove widespread Neoglacial advance through the combined effect of
606 increased winter snowfall under a generally cooler regime, yielding a marked regional
607 positive mass balance perturbation. In particular, we note during the past millennium three
608 intervals of lower $\delta^{18}\text{O}_{\text{diatom}}$ values between 1275–1350 AD, 1400–1550 AD, and 1700–1850
609 AD coincide with three well-documented episodes of Little Ice Age (LIA) glacier advance on
610 mainland Alaska (Fig. 5 and 7) [*Calkin et al. 2001; Solomina et al. 2015*]. Furthermore, the
611 $\delta^{18}\text{O}_{\text{diatom}}$ minimum at 1805 AD (+24.6 ‰) marks the culmination of regional LIA glacial

612 advance [*Barclay et al.* 2009; *Calkin et al.* 2001; *Wiles et al.* 2004; *Solomina et al.* 2015]
613 (Fig. 5 and 7).

614

615 **5.4 Paleoisotopic coherence and atmospheric circulation**

616 Several paleoisotope records from Alaska have also been interpreted in terms of synoptic-
617 scale changes in atmospheric circulation and inter-comparison with Heart Lake $\delta^{18}\text{O}_{\text{diatom}}$
618 yields many commonalities and insights [*Anderson et al.* 2005; *Fisher et al.* 2004; 2008;
619 *Schiff et al.* 2009; *Jones et al.* 2014; *Hammarlund et al.* 2015] (Fig. 7). For instance, a strong
620 inverse relationship *ca.* 9.5–4.0 ka is apparent with millennial scale $\delta^{18}\text{O}_{\text{diatom}}$ variations at
621 Mica Lake, in Prince William Sound [*Schiff et al.* 2009] (Fig. 7). Lower Mica Lake $\delta^{18}\text{O}_{\text{diatom}}$
622 values indicate precipitation delivered by zonal flow under a weak Aleutian Low, whereby
623 precipitating systems are subject to increased rainout as they pass over the Kenai Peninsula
624 and coastal mountain ranges. Conversely, increased meridional flow during a strong Aleutian
625 Low delivers locally sourced moisture from nearby Gulf of Alaska, thereby reducing
626 distillation and isotope depletion in precipitation, thus yielding higher Mica Lake $\delta^{18}\text{O}_{\text{diatom}}$
627 values [*Schiff et al.* 2009]. The reciprocal relationship between precipitation-inferred $\delta^{18}\text{O}$
628 values at Heart and Mica Lakes between *ca.* 9.5–4.0 ka conforms to modelling and empirical
629 analyses of spatial patterns of $\delta^{18}\text{O}_{\text{P}}$ [*Berkelhammer et al.* 2012; *Bailey et al.* 2015]. The
630 Horse Trail Fen record from the Kenai lowlands is also comparable to Heart Lake from *ca.*
631 8.0 ka and demonstrates overall higher $\delta^{18}\text{O}$ values during the early Holocene and reflecting
632 generally weak Aleutian Low circulation [*Jones et al.* 2014]. The only other full Holocene
633 paleoisotope record from eastern Beringia is from the Mount Logan ice core [*Fisher et al.*
634 2008], which exhibits strong correspondence with the Jellybean [*Anderson et al.* 2005] and
635 Heart Lake $\delta^{18}\text{O}$ records during the early-mid Holocene (Fig. 7).

636 Secondary, but notable departures between paleoisotope records are evident during
637 the late Holocene (Fig. 7), some of which can be reconciled by considering the detailed, non-

638 linear complexity of atmospheric circulation. For instance between *ca.* 3.0–1.0 ka Heart Lake
639 $\delta^{18}\text{O}_{\text{diatom}}$ does not exhibit marked excursions to the higher $\delta^{18}\text{O}$ values documented in Mt.
640 Logan, Jellybean and Pechora Lakes, interpreted as an interval of pronounced weak Aleutian
641 Low circulation [Anderson *et al.* 2005; Fisher *et al.* 2008; Hammarlund *et al.* 2015]. At Heart
642 Lake, this period is characterized by $\delta^{18}\text{O}_{\text{diatom}}$ values closer to the Holocene mean (Fig. 7).
643 These differences could reflect prevailing atmospheric patterns characterized by a more
644 southerly displaced western centre of low pressure in the northwest Pacific, which typically
645 results in a higher density of storms being steered into the Gulf of Alaska and eastern
646 Kamchatka Peninsula [Mock *et al.* 1998; Rodionov *et al.* 2007]. Under such conditions,
647 precipitation at Mt. Logan, Jellybean and Pechora Lakes would be relatively ^{18}O -enriched
648 [Berkelhammer *et al.* 2012], whereas Heart Lake would fail to exhibit higher $\delta^{18}\text{O}_{\text{diatom}}$ values
649 since these storm systems would track south of the Aleutian Islands [Rodionov *et al.* 2007].

650

651 **6. Conclusions**

652 The datasets and analysis presented here extend modern observations across Alaska and
653 Siberia back through the Holocene to bridge a critical gap in the regional network of proxy-
654 climate records required to assess the complex spatio-temporal patterns of past North Pacific
655 climate change [Sundqvist *et al.* 2014; Brooks *et al.* 2015; Kaufman *et al.* 2016]. We show
656 that atmospheric circulation across the North Pacific exerted the dominant control on both
657 local and regional environmental conditions from the early Holocene through to the present
658 day. Although GCMs typically emphasize insolation as the key driver of Holocene
659 temperature change in Alaska [Renssen *et al.* 2009], we demonstrate a more complex
660 relationship and emphasise the role of moisture availability and transport within the
661 land–atmosphere–ocean system. In particular, shifts in Aleutian Low circulation directly
662 impacted the net mass balance of south-central Alaska’s glaciers and ice fields through
663 temperature and precipitation variability [Solomina *et al.* 2015]. Given that Alaska is

664 currently experiencing a period of intensified Aleutian Low circulation, which should be
665 favourable for glacier *growth*, the widespread and well documented 21st century retreat of
666 glaciers and ice cover [Larsen *et al.* 2015] would now appear to be unprecedented within the
667 context of long-term Holocene environmental change.

668 **7. Acknowledgements**

669 The US Fish and Wildlife Service, Alaska Maritime Natural Wildlife Refuge and CPS Polar
670 services provided logistical support and access for fieldwork on Adak Island. This research
671 was funded by NSF award EAR 0823522, NERC grants IP/1202/1110 and IP/1460/0514, and
672 a NERC CASE award to H.L.B. (NE/I528350/1). We thank Yarrow Axford, Anne Krawiec,
673 Caleb Schiff, and David Vaillencourt for their field assistance. H.L.B. acknowledges a
674 Lloyds of London Fulbright Scholar award for funding during the preparation of this
675 manuscript. A.L.H. acknowledges a Research Professorship funded by the Research Council
676 of Norway through its Centres of Excellence (Grant 223259).

677

678 **8. Data availability**

679 Key datasets for this study are available in Supplementary Table 1. All data produced by this
680 study (*will be*) available online at the World Data Center for Paleoclimatology (WDC Paleo)
681 (<https://www.ncdc.noaa.gov/data-access/paleoclimatology-data>) and in the NERC National
682 Data Repository.

683

684 **9. References**

685 Anderson, L., Abbot, M.B., Finney, B.P., and Burns, S.J., (2005), Regional atmospheric
686 circulation change in the North Pacific during the Holocene inferred from lacustrine
687 carbonate oxygen isotopes, Yukon Territory, Canada, *Quat. Res.*, 64, 21–35, doi:
688 10.1016/j.yqres.2005.03.005.

689 Anderson, R.S., Hallett, D.J., Berg, E., Jass, R.B., Toney, J.L., De Fontaine, C.S., and
690 DeVolder, A., (2006), Holocene development of boreal forests and fire regimes on the Kenai
691 Lowlands of Alaska, *The Holocene*, 16(6), 791–803, doi: 10.1191/0959683606hol966rp.

692 Anderson, L., Berkelhammer, M., Barron, J.A., Steinman, B.A., Finney, B.P., and Abbott,
693 M.B., (2016), Lake oxygen isotopes as recorders of North American Rocky Mountain
694 hydroclimate: Holocene patterns and variability at multi-decadal to millennial timescales,
695 *Glob. Planet. Change*, 137, 131–148, doi: 10.1016/j.gloplacha.2015.12.021.

696 Andrén, E., Klimaschewski, A., Self, A. E., Amour, N. S., Andreev, A. A., Bennett, K. D.,
697 Conley, D.J., Edwards, T.W.D., Solovieva, N., and Hammarlund, D., (2015), Holocene
698 climate and environmental change in north-eastern Kamchatka (Russian Far East), inferred
699 from a multi-proxy study of lake sediments, *Global Planet. Change*, 134, 41–54, doi:
700 10.1016/j.gloplacha.2015.02.013.

701 Baier, J., Lücke, A., Negendank, J.F., Schleser, G.H., and Zolitschka, B., (2004), Diatom and
702 geochemical evidence of mid-to late Holocene climatic changes at Lake Holzmaar, West-
703 Eifel (Germany), *Quat. Int.*, 113(1), 81–96, doi: 10.1016/S1040-6182(03)00081-8.

704 Bailey, H.L., Henderson, A.C.G., Sloane, H.J., Snelling, A., Leng, M.J., and Kaufman, D.S.,
705 (2014), The effects of species on lacustrine $\delta^{18}\text{O}_{\text{diatom}}$ and its implications for environmental
706 reconstructions, *J. Quat. Sci.*, 29, 393–400, doi: 10.1002/jqs.2711.

707 Bailey, H.L., Kaufman, D.S., Henderson, A.C.G., and Leng, M.J., (2015), Synoptic scale
708 controls on the $\delta^{18}\text{O}$ in precipitation across Beringia, *Geophys. Res. Lett.*, 42, 4608–4616,
709 doi: 10.1002/2015GL063983.

710 Barclay, D.J., Wiles, G.C., and Calkin, P.E., (2009), Holocene glacier fluctuations in Alaska,
711 *Quat. Sci. Rev.*, 28, 2034–2048, doi: 10.1016/j.quascirev.2009.01.016.

712 Barker, P.A., Street-Perrott, F.A., Leng, M.J., Greenwood, P.B., Swain, D.L., Perrott, R.A.,
713 Telford, J., and Ficken, K.J., (2001) A 14 ka oxygen isotope record from diatom silica in two
714 alpine tarns on Mt. Kenya, *Science*, 292, 2307–2310, doi: 10.1126/science.1059612.

715 Barr, I.D., and Solomina, O., (2014), Pleistocene and Holocene glacier fluctuations upon the
716 Kamchatka Peninsula, *Glob. Planet Change*, 113, 110-120, doi:
717 10.1016/j.gloplacha.2013.08.005.

718 Berger, A., and Loutre, M.F., (1991), Insolation values for the climate of the last 10 million
719 years, *Quat. Sci. Rev.*, 10, 297–317, doi:10.1016/0277-3791(91)90033-Q.

720 Berkelhammer, M., Stott, L., Yoshimura, K., Johnson, K., and Sinha, A., (2012), Synoptic
721 and mesoscale controls on the isotopic composition of precipitation in the western United
722 States, *Climate Dynamics*, 38 (3-4), 433–454, doi: 10.1007/s00382-011-1262-3.

723 Biskaborn, B.K., Subetto, D.A., Savelieva, L.A., Vakhrameeva, P.S., Hansche, A.,
724 Herzsuh, U., Klemm, J., Heinecke, L., Pestryakova, L.A., Meyer, H., and Kuhn, G.,
725 (2016), Late Quaternary vegetation and lake system dynamics in north-eastern Siberia:
726 Implications for seasonal climate variability, *Quat. Sci. Rev.*, 147, 406–421, doi:
727 10.1016/j.quascirev.2015.08.014.

728 Black, R.F., (1976), Late Quaternary glacial events, Aleutian Islands, Alaska. In:
729 Easterbrook, D.D., Sibrava, V. (Eds.), *Quaternary Glaciations in the Northern Hemisphere*.
730 IUGSUNESCO International Geological Correlations Program, Project 73-1-24. International
731 Union of Quaternary Research, Bellingham, pp. 285–301.

732 Bradbury, P., Cumming, B., and Laird, K., (2002), A 1500-year record of climatic and
733 environmental change in Elk Lake, Minnesota III: measures of past primary productivity, *J.*
734 *Paleolimnol.*, 27(3), 321–340, doi: 10.1023/A:1016035313101.

735 Bradley, C.C., (1948), Geologic notes on Adak Island and the Aleutian chain, Alaska, *Am. J.*
736 *Sci.*, 246(4), 214-240, doi: 10.2475/ajs.246.4.214.

737 Brooks, S.J., Diekmannb, B., Jones, V.J., and Hammarlund, D., (2015), Holocene
738 environmental change in Kamchatka: A synopsis, *Glob. Planet Change*, 134, 166–174, doi:
739 10.1016/j.gloplacha.2015.09.004.

740 Calkin, P.E., Wiles, G.C., and Barclay, D. J., (2001), Holocene coastal glaciation of Alaska,
741 *Quat. Sci. Rev.*, 20, 449–461, doi: 10.1016/S0277-3791(00)00105-0.

742 Camburn, K.E., and Charles, D.F., (2000), *Diatoms of Low-alkalinity Lakes in the*
743 *Northeastern United States*, ANSP Special Publication 18. Academy of Natural Sciences of
744 Philadelphia, Philadelphia.

745 Cavalieri, D.J., and Parkinson, C.L., (1987), On the relationship between atmospheric
746 circulation and the fluctuations in the sea ice extents of the Bering and Okhotsk Seas, *J.*
747 *Geophys. Res.*, 92, 7141–7162, doi: 10.1029/JC092iC07p07141.

748 Chaplign, B., Narancic, B., Meyer, H., and Pienitz, R., (2016), Paleo-environmental
749 gateways in the eastern Canadian arctic—Recent isotope hydrology and diatom oxygen
750 isotopes from Nettilling Lake, Baffin Island, Canada, *Quat. Sci. Rev.*, 147, 379–390, doi:
751 10.1016/j.quascirev.2016.03.028.

752 Clayton, R.N., and Mayeda, T.K., (1963), The use of bromine pentafluoride in the extraction
753 of oxygen from oxide and silicates for isotopic analysis, *Geochim. Cosmochim. Acta*, 27, 43–
754 52, doi: 10.1016/0016-7037(63)90071-1.

755 Clegg, B.F., and Hu, F.S., (2010), An oxygen-isotope record of Holocene climate change in
756 south-central Brooks Range, Alaska, *Quat. Sci. Rev.*, 29, 928–939, doi:
757 10.1016/j.quascirev.2009.12.009.

758 Coats, R.R., (1956), *Reconnaissance geology of some western Aleutian Islands, Alaska*, US
759 Geological Survey Bulletin 1028-E, Government Printing Office.

760 Corbett, D., West, D., and Lefevre, C., (2010), *The People at the End of the World: The*
761 *Western Aleutian Project and the Archeology of Shemya Island*, Alaska Anthropological
762 Association Monograph Series VIII.

763 Devlin, J.E., and Finkelstein, S.A., (2011), Local physiographic controls on the responses of
764 Arctic lakes to climate warming in Sirmilik National Park, Nunavut, Canada, *J. Paleolimnol.*,
765 45(1), 23–39, doi: 10.1007/s10933-010-9477-6.

766 Douglas, M.S.V., and Smol, J.P., (2010), *Freshwater diatoms as indicators of environmental*
767 *change in the High Arctic*, In: Smol, J.P., Stoermer, E.F. (Eds.), *The Diatoms: Application for*
768 *the Environmental and Earth Sciences*. Cambridge University Press, Cambridge, pp.
769 249–266.

770 Fisher, D.A., Wake, C., Kreutz, K., Yalcin, K., Steig, E., Mayewski, P., Anderson, L., Zheng,
771 J., Rupper, S., Zdanowicz, C., Demuth, M., Waszkiewicz, M., Dahl-Jensen, D., Goto-Azuma,
772 K., Bourgeois, J.B., Koerner, R.M., Sekerka, J., Osterberg, E., Abbott, M.B., Finney, B.P.,
773 and Burn, S.J., (2004), Stable isotope records from Mount Logan, Eclipse ice cores and
774 nearby Jellybean Lake. Water cycle of the North Pacific over 2000 years and over five
775 vertical kilometres: Sudden shifts and tropical connections, *Geogr. Phys. Quat.*, 58 (2–3),
776 337–352, doi: 10.7202/013147ar.

777 Fisher, D., Osterberg, E., Dyke, A., Dahl-Jensen, D., Demuth, M., Zdanowicz, C., Bourgeois,
778 J., Koerner, R.M., Mayewski, P., Wake, C., Kreutz, K., Steig, E., Zheng, J., Yalcin, K., Goto-
779 Azuma, K., Luckman B., and Rupper, S., (2008), The Mt Logan Holocene-late Wisconsinan
780 isotope record: tropical Pacific--Yukon connections, *The Holocene*, 18, 667–677, doi:
781 10.1177/0959683608092236.

782 Fraser, G.D., and Snyder, G.L., (1959), *Geology of southern Adak Island and Kagalska*
783 *Island, Alaska*, US Geological Survey Bulletin 1028, pp. 371–408.

784 Gibson, C.E., Anderson, N.J., and Haworth, E.Y., (2003), *Aulacoseira subarctica*: taxonomy,
785 physiology, ecology and palaeoecology, *Eur. J. Phycol.*, 38, 83–101, doi:
786 10.1080/0967026031000094102.

787 Grimm, E.C., (1987), Coniss - a Fortran-77 program for stratigraphically constrained cluster-
788 analysis by the method of incremental sum of squares. *Comput. Geosci.*, 13, 13–35.

789 Grimm, E.C., (2015) TILIA software. Version 2.0.41. <https://www.tiliait.com/download/>

790 Hammarlund, D., Klimaschewski, A., St. Amour, N.A., Andrén, E., Self, A.E., Solovieva, N.,
791 Andreev, A.A., Barnekowa, L., and Edwards, T.W.D, (2015), Late Holocene expansion of
792 Siberian dwarf pine (*Pinus pumila*) in Kamchatka in response to increased snow cover as
793 inferred from lacustrine oxygen-isotope records, *Glob. Planet. Change*, 134, 91–100, doi:
794 10.1016/j.gloplacha.2015.04.004.

795 Harada, N., Katsuki, K., Nakagawa, M., Matsumoto, A., Seki, O., Addison, J.A., Finney,
796 B.P., and Sato, M., (2014), Holocene sea surface temperature and sea ice extent in the
797 Okhotsk and Bering Seas, *Prog. Oceanogr.*, 126, 242–253, doi:
798 10.1016/j.pocean.2014.04.017.

799 Hausmann, S., and Pienitz, R., (2009), Seasonal water chemistry and diatom changes in six
800 boreal lakes of the Laurentian Mountains (Québec, Canada): impacts of climate and timber
801 harvesting, *Hydrobiologia*, 635(1), 1–14, doi: 10.1007/s10750-009-9855-0.

802 Heusser, C.J., (1978), Post-glacial vegetation on Adak Island, Aleutian Islands, Alaska. *Bull.*
803 *Torrey Bot. Club.*, 105, 18–23, doi: 10.2307/2484259.

804 Hoff, U., Biskaborn, B.K., Dirksen, V.G., Dirksen, O., Kuhn, G., Meyer, H., Nazarova, L.,
805 Roth, A., and Diekmann, B., (2015), Holocene environment of Central Kamchatka, Russia:
806 Implications from a multi-proxy record of Two-Yurts Lake, *Glob. Planet. Change*, 134,
807 101–117, doi: 10.1016/j.gloplacha.2015.07.011.

808 Horn, H., Paul, L., Horn, W., and Petzoldt, T., (2011), Long-term trends in the diatom
809 composition of the spring bloom of a German reservoir: is *Aulacoseira subarctica* favoured
810 by warm winters? *Fresh. Biol.*, 56(12), 2483–2499, doi: 10.1111/j.1365-2427.2011.02674.x.

811 IAEA/WMO, (2017), *Global Network of Isotopes in Precipitation*, The GNIP Database.
812 Accessible at: <http://www.iaea.org/water>.

813 Interlandi, S.J., Kilham, S.S., and Theriot, E.C., (1999), Responses of phytoplankton to
814 varied resource availability in large lakes of the Greater Yellowstone Ecosystem, *Limnol.*
815 *Oceanogr.*, 44(3), 668–682, doi: 10.4319/lo.1999.44.3.0668.

816 Itaki, T., and Ikehara, K., (2004), Middle to late Holocene changes of the Okhotsk Sea
817 Intermediate Water and their relation to atmospheric circulation, *Geophys. Res. Lett.*, 31,
818 L24309, doi: 10.1029/2004GL021384.

819 Jones, V.J., Leng, M.J., Solovieva, N., Sloane, H.J. and Tarasov, P., (2004) Holocene climate
820 of the Kola Peninsula; evidence from the oxygen isotope record of diatom silica, *Quat. Sci.*
821 *Rev.*, 23(7–8), 833–839, doi: 10.1016/j.quascirev.2003.06.014.

822 Jones, M. C., Wooller, M., and Peteet, D.M., (2014), A deglacial and Holocene record of
823 climate variability in south-central Alaska from stable oxygen isotopes and plant macrofossils
824 in peat, *Quat. Sci. Rev.*, 87, 1–11, doi: 10.1016/j.quascirev.2013.12.025.

825 Juggins, S., (2014), C2 Data Analysis. Version 1.7.6. University of Newcastle, Newcastle.

826 Kalnay, E. *et al.* (1996), The NCEP/NCAR 40-Year Reanalysis Project. *Bull. Am. Meteorol.*

827 *Soc.*, 77, 437–471.

828 Kaufman, D.S., Ager, T.A., Anderson, N.J., Anderson, P.M., Andrews, J.T., Bartelein, P.J.,
829 Burbaker, L.B., Coats, L.L., Cwynar, L.C., Duval, M.L., Dyke, A.S., Edwards, M.E., Eiser,
830 W.R., Gajewski, K., Geisodottir, A., Hu, F.S., Jennings, A.E., Kaplan, M.R., Kewin, M.W.,
831 Lozhkin, A.V., MacDonald, G.M., Miller, G.H., Mock, C.J., Oswald, W.W., Otto-Blisner,
832 B.L., Porinchu, D.F., Rühland, K., Smol, J.P., Steig, E.J., and Wolfe, B.B., (2004), Holocene
833 thermal maximum in the western Arctic (0-180° W), *Quat. Sci. Rev.*, 23, 529–560, doi:
834 10.1016/j.quascirev.2003.09.007.

835 Kaufman, D.S., Axford, Y.L., Henderson, A.C.G., McKay, N.P., Oswald, W.W., Saenger, C.,
836 Anderson, R.S., Bailey, H.L., Clegg, B., Gajewski, K., Sheng Hu, F., Jones, M.C., Massa, C.
837 Routson, C.C., Werner, A., Wooller, M.J., and Yu, Z., (2016), Holocene climate changes in
838 eastern Beringia (NW North America) — A systematic review of multi-proxy evidence,
839 *Quat. Sci. Rev.*, 147, 312–339, doi: 10.1016/j.quascirev.2015.10.021.

840 Krammer, K., and Lange-Bertalot, H., (1986–1991), *Bacillariophyceae Band 2/2*. Gustav
841 Fischer Verlag, Stuttgart, pp.1–4.

842 Krawiec, A.C.L., and Kaufman, D.S., (2014), Holocene storminess inferred from sediments of
843 two lakes on Adak Island, Alaska, *Quaternary Res.*, 82, 73–84, doi:
844 10.1016/j.yqres.2014.02.007.

845 Krawiec, A.C.L., Kaufman, D.S., and Vaillencourt, D.A., (2013), Age models and
846 tephrostratigraphy from two lakes on Adak Island, Alaska. *Quat. Geochronol.*, 18, 41–53,
847 doi: 10.1016/j.quageo.2013.07.002.

848 Labeyrie, L.D., (1974), New approach to surface seawater palaeotemperatures using $^{18}\text{O}/^{16}\text{O}$
849 ratios in silica of diatom frustules, *Nature*, 248, 40–42, doi: 10.1038/248040a0.

850 Lachniet, M.S., Lawson, D.E., Stephen, H., Sloat, A.R., and Patterson, W.P., (2016),
851 Isoscapes of $\delta^{18}\text{O}$ and $\delta^2\text{H}$ reveal climatic forcings on Alaska and Yukon precipitation, *Water*
852 *Resour. Res.*, 52(8), 6575–6586, doi: 10.1002/2016WR019436.

853 Lamb., A.L., Brewer, T.S., Leng, M.J., Sloane, H.J., and Lamb, H.F., (2007), A geochemical
854 method for removing the effect of tephra on lake diatom oxygen isotope records, *J.*
855 *Paleolimnol.*, 37, 499–516, doi: 10.1007/s10933-006-9034-5.

856 Larsen, C.F., Burgess, E., Arendt, A.A., O'neel, S., Johnson, A.J. and Kienholz, C., (2015),
857 Surface melt dominates Alaska glacier mass balance, *Geophys. Res. Lett.*, 42(14),
858 5902–5908, doi: 10.1002/2015GL064349. .

859 Leclerc, A.J., and Labeyrie, L., (1987), Temperature dependence of the oxygen isotopic
860 fractionation between diatom silica and water, *Earth Planet. Sci. Lett.*, 84(1), 69–74, doi:
861 10.1016/0012-821X(87)90177-4.

862 Leng, M.J., and Barker, P.A., (2006), A review of the oxygen isotope composition of
863 lacustrine diatom silica for paleoclimate reconstruction, *Earth Sci. Rev.*, 75, 5–27, doi:
864 10.1016/j.earscirev.2005.10.001.

865 Leng, M.J., and Sloane, H.J., (2008), Combined oxygen and silicon isotope analysis of
866 biogenic silica, *J. Quat. Sci.*, 23, 313–319, doi: 10.1002/jqs.1177.

867 Leng, M., Barker, P., Greenwood, P., Roberts, N., and Reed, J., (2001), Oxygen isotope
868 analysis of diatom silica and authigenic calcite from Lake Pinarbasi, Turkey, *J. Paleolimnol.*,
869 25(3), 343–349, doi: 10.1023/A:1011169832093.

870 Lepskaya, E.V., Jewson, D.H., and Usoltseva, M.V., (2010), *Aulacoseira subarctica* in
871 Kurilskoye Lake, Kamchatka: a deep, oligotrophic lake and important Pacific salmon
872 nursery, *Diatom Research*, 25(2), 323–335, doi: 10.1080/0269249X.2010.9705853.

873 Lotter, A.F., and Bigler, C., (2000), Do diatoms in the Swiss Alps reflect the length of
874 ice-cover? *Aquatic Sciences*, 62(2), 125–141, doi: 10.1007/s000270050002.

875 Lotter, A.F., Pienitz, R., and Schmidt, R., (2010), *Diatoms as indicators of environmental*
876 *change in subarctic and alpine regions*, In: Smol, J.P., Stoermer, E.F. (Eds.), *The Diatoms:*
877 *Application for the Environmental and Earth Sciences*. Cambridge University Press,
878 Cambridge.

879 Mackay, A.W., Swann, G.E.A., Brewer, T.S., Leng, M.J., Morley, D.W., Piotrowska, N.,
880 Rioual, P., and White, D., (2011), A reassessment of late glacial—Holocene diatom oxygen
881 isotope record from Lake Baikal using a geochemical mass-balance approach, *J. Quat. Sci.*
882 26, 627–634, doi: 10.1002/jqs.1484.

883 Mantua, N.J., Hare, S.R., Zhang, Y., Wallace, J.M., and Francis, R.C., (1997), A Pacific
884 interdecadal climate oscillation with impacts on salmon production, *Bull. Am. Meteorol. Soc.*,
885 78, 1069–1079, doi: 10.1175/1520-0477(1997)078<1069:APICOW>2.0.CO;2.

886 Marcott, S.A., Shakun, J.D., Clark, P.U., and Mix, A.C., (2013), A reconstruction of regional
887 and global temperature for the past 11 300 years, *Science*, 339, 1198–1201, doi:
888 10.1126/science.1228026.

889 Max, L., Riethdorf, J-R., Tiedemann R., Smirnova, M., Lembke-Jene, L., Fahl, K., Nürnberg,
890 D., Matul, A., and Mollenhauer, G., (2012), Sea surface temperature variability and sea-ice
891 extent in the subarctic northwest Pacific during the past 15,000 years, *Paleoceanography*, 27,
892 PA3213, doi:10.1029/2012PA002292.

893 Mayewski, P.A., Rohling, E.E., Stager, J.C., Karlén, K.A., Maasch, W., Meeker, L.D.,
894 Meyerson, E.A., Gasse, F., van Kreveld, S., Holmgren, K., Lee-Thorp, J., Rosqvist, G., Rack,

895 F., Staubwasser, M., Schneider, R.R., and Steiger, E.J., (2004), Holocene climate variability,
896 *Qual. Res.*, 62, 243–255, doi: 10.1016/j.yqres.2004.07.001.

897 Meyer, H., Chaplignin, B., Hoff, U., Nazarova, L., and Diekmann, B., (2015), Oxygen isotope
898 composition of diatoms as Late Holocene climate proxy at Two-Yurts-Lake, Central
899 Kamchatka, Russia. *Glob. Planet. Chang.*, 134, 118–128, doi:
900 10.1016/j.gloplacha.2014.04.008.

901 Minoshima, K., Kawahata, H., and Ikehara, K., (2007), Changes in biological production in
902 the mixed water region (MWR) of the northwestern North Pacific during the last 27 kyr,
903 *Palaeogeogr. Palaeoclimatol. Palaeoecol.*, 254, 430–447, doi:10.1016/j.palaeo.2007.06.022.

904 Mock, C. J., Bartlein, P. J., and Anderson, P. M., (1998), Atmospheric circulation patterns
905 and spatial climatic variations in Beringa, *Int. J. Climatol.*, 10, 1085–1104,
906 doi:10.1002/(SICI)1097-0088(199808)18:10<1085::AID-JOC305>3.0.CO;2-K.

907 Morley, D.W., Leng, M.J., Mackay, A.W., Sloane, H.J., Rioual, P. and Battarbee, R.W.,
908 (2004), Cleaning of lake sediment samples for diatom oxygen isotope analysis, *J.*
909 *Paleolimnol.*, 31(3), 391–401, doi: 10.1023/B:JOPL.0000021854.70714.6b.

910 Nazarova, L., de Hoog, V., Hoff, U., Dirksen, O., and Diekmann, B., (2013), Late Holocene
911 climate and environmental changes in Kamchatka inferred from the subfossil chironomid
912 record, *Quat. Sci. Rev.*, 67, 81–92, doi: 10.1016/j.quascirev.2013.01.018.

913 NOAA, (2017), National Oceanic and Atmospheric Administration. National Climatic Data
914 Centre. <https://www.ncdc.noaa.gov/land-based-station-data>.

915 Rehfeld, K., Münch, T., Ho, S.L., and Laepple, T., (2018), Global patterns of declining
916 temperature variability from the Last Glacial Maximum to the Holocene, *Nature*, 554 (7692),
917 356–359, doi:10.1038/nature25454.

918 Renssen, H., Seppä, H., Heiri, O., Goosse, H., and Fichefet, T., (2009), The spatial and
919 temporal complexity of the Holocene thermal maximum, *Nat. Geosci.*, 2, 411–414, doi:
920 10.1038/ngeo513.

921 Renssen, H., Seppä, H., Crosta, X., Goosse, H., and Roche, D.M., (2012), Global
922 characterization of the Holocene Thermal Maximum, *Quat. Sci. Rev.*, 48, 7–19, doi:
923 10.1016/j.quascirev.2012.05.022.

924 Rioual, P., Andrieu-Ponel, V., Rietti-Shati, M., Battarbee, R.W., de Beaulieu, J.L., Cheddadi,
925 R., Reille, M., Svobodova, H., and Shemesh, A., (2001), High-resolution record of climate
926 stability in France during the last interglacial period, *Nature*, 413(6853), 293–296, doi:
927 10.1038/35095037.

928 Rioual, P., Andrieu-Ponel, V., de Beaulieu, J.L., Reille, M., Svobodova, H., and Battarbee,
929 R.W., (2007), Diatom responses to limnological and climatic changes at Ribains Maar
930 (French Massif Central) during the Eemian and Early Würm, *Quat. Sci. Rev.*, 26(11),
931 1557–1609, doi: 10.1016/j.quascirev.2007.03.009.

932 Roberts, S., Jones, V.J., Allen, J.R., and Huntley, B., (2015), Diatom response to mid-
933 Holocene climate in three small Arctic lakes in northernmost Finnmark, *The Holocene*, 25(6),
934 911–920, doi: 10.1177/0959683615572853.

935 Rodionov, S. N., Bond, N.A., and Overland, J.E., (2007), The Aleutian Low, storm tracks,
936 and winter climate variability in the Bering Sea, *Deep Sea Res. II.*, 54, 2560–2577, doi:
937 10.1016/j.dsr2.2007.08.002.

938 Rosqvist, G., Jonsson, C., Yam, R., Karlén, W., and Shemesh, A., (2004), Diatom oxygen
939 isotopes in pro-glacial lake sediments from northern Sweden: a 5000 year record of
940 atmospheric circulation, *Quat. Sci. Rev.*, 23(7), 851–859, doi:
941 10.1016/j.quascirev.2003.06.009.

942 Rühland, K., Priesnitz, A., and Smol, J.P., (2003), Paleolimnological evidence from diatoms
943 for recent environmental changes in 50 lakes across Canadian Arctic treeline, *Arct. Antarct.*
944 *Alp. Res.*, 35(1), 110–123, doi: 10.1657/1523-0430(2003)035[0110:PEFDFR]2.0.CO;2.

945 Rühland, K., Paterson, A.M., and Smol, J.P., (2008), Hemispheric-scale patterns of climate-
946 related shifts in planktonic diatoms from North American and European lakes, *Glob. Change*
947 *Biol.*, 14(11), 2740–2754, doi: 10.1111/j.1365-2486.2008.01670.x.

948 Saros, J.E. and Anderson, N.J., 2015. The ecology of the planktonic diatom *Cyclotella* and its
949 implications for global environmental change studies, *Biol. Rev.*, 90(2), 522–541, doi:
950 10.1111/brv.12120.

951 Savoskul, O.S., (1999), Holocene glacier advances in the headwaters of Sredniaya Avacha,
952 Kamchatka, Russia, *Qual. Res.*, 52, 14–26, doi: 10.1006/qres.1999.2051.

953 Schiff, C.J., Kaufman, D.S., Wolfe, A.P., Dodd, J., and Sharp, Z., (2009), Late Holocene
954 storm-trajectory changes inferred from the oxygen isotope composition of lake diatoms, south
955 Alaska, *J. Paleolimnol.*, 41, 189–208, doi: 10.1007/s10933-008-9261-z.

956 Smol, J. P., Wolfe, A. P., Birks, H. J. B., Douglas, M. S., Jones, V. J., Korhola, A., Pienitz,
957 R., Rühland, K., Sorvari, S., Antoniades, D., and Brooks, S. J., (2005), Climate-driven regime
958 shifts in the biological communities of arctic lakes., *PNAS*, 102(12), 4397–4402, doi:
959 10.1073/pnas.0500245102.

960 Solomina, O.N., Bradley, R.S., Hodgson, D.A., Ivy-Ochs, S., Jomelli, V., Macintosh, A.N.,
961 Nesje, A., Owen, L.A., Wanner, H., Wiles, G.C., and Young, N.E., (2015), Holocene glacier
962 fluctuations, *Quat. Sci. Rev.*, 111, 9–34, doi: 10.1016/j.quascirev.2014.11.018.

963 Solovieva, N., Klimaschewski, A., Self, A. E., Jones, V. J., Andrén, E., Andreev, A. A.,
964 Hammarlund, D., Lepskaya, E.V., and Nazarova, L., (2015), The Holocene environmental

965 history of a small coastal lake on the north-eastern Kamchatka Peninsula, *Glob. Planet.*
966 *Change*, 134, 55–66, doi: 10.1016/j.gloplacha.2015.06.010.

967 Spaulding, S.A., Lubinski, D.J. and Potapova, M., (2017), Diatoms of the United States.
968 <http://westerndiatoms.colorado.edu>

969 Streletskiy, D.A., Tananaev, N.I., Opel, T., Shiklomanov, N.I., Nyland, K.E., Streletskaya,
970 I.D. and Shiklomanov, A.I., (2015), Permafrost hydrology in changing climatic conditions:
971 seasonal variability of stable isotope composition in rivers in discontinuous permafrost.
972 *Environ. Res. Lett.*, 10 (9), p.095003, doi: 10.1088/1748-9326/10/9/095003.

973 Sundqvist, H.S., Kaufman, D.S., McKay, N.P., Balascio, N.L., Briner, J.P., Cwynar, L.C.,
974 Sejrup, H.P., Seppä, H., Subetto, D.A., Andrews, J.T. and Axford, Y., (2014), Arctic
975 Holocene proxy climate database—new approaches to assessing geochronological accuracy
976 and encoding climate variables *Clim. Past*, 10(4), 1605–1631, doi: 10.5194/cp-10-1605-
977 2014.

978 Swann, G.E.A., and Patwardhan, S.V., (2011), Application of Fourier Transform Infrared
979 Spectroscopy (FTIR) for assessing biogenic silica sample purity in geochemical analyses and
980 palaeoenvironmental research, *Clim. Past*, 7, 65–74, doi: 10.5194/cp-7-65-2011.

981 TDX (2013), TDX Power - Adak Reconnaissance Study. *Hatch*.
982 <http://akenergyinventory.org/hyd/SSH-2013-0004.pdf>

983 ter Braak, C.J.F., and Prentice, I.C., (1988), A theory of gradient analysis, *Adv. Ecol. Res.*,
984 18, 271–317, doi: 10.1016/S0065-2504(03)34003-6.

985 Trenberth, K.E., and Hurrell, J.W., (1994), Decadal atmosphere-ocean variations in the
986 Pacific, *Clim. Dyn.*, 9, 303–319, doi: 10.1007/BF00204745.

987 USGS, (2017), USGS Landsat 8 Images. Available at: <https://landsat.gsfc.nasa.gov/>

988 Vachula, R.S., Chipman, M.L., and Hu, F.S., (2017), Holocene climatic change in the
989 Alaskan Arctic as inferred from oxygen-isotope and lake-sediment analyses at Wahoo Lake,
990 *The Holocene*, 27 (4), 1–14, doi: <https://doi.org/10.1177/0959683617702230>.

991 Walker, M., Berhelhammer, M., Björck, S., Cwynar, L.C., Fisher, D.A., Long, A.J., Lowe,
992 J.J., Newnham, R.M., Rasmussen, S.O., and Weis, H., (2012), Formal subdivision of the
993 Holocene Series/Epoch: a discussion Paper by a Working Group of INTIMATE (Integration
994 of ice-core, marine and terrestrial records) and the Subcommittee on Quaternary
995 Stratigraphy (International Commission on Stratigraphy), *J. Quat. Sci.*, 27, 649–659, doi:
996 10.1002/jqs.2565.

997 Wang, L., Lu, H., Liu, J., Gu, Z., Mingram, J., Chu, G., Li, J., Rioual, P., Negendank, J.F.,
998 Han, J., and Liu, T., (2008), Diatom-based inference of variations in the strength of Asian
999 winter monsoon winds between 17,500 and 6000 calendar years BP, *J. Geophys. Res. Atmos.*,
1000 113, D2101, doi: 10.1029/2008JD010145.

1001 Welker, J.M., (2000), Isotopic ($\delta^{18}\text{O}$) characteristics of weekly precipitation collected
1002 across the USA: an initial analysis with application to water source studies, *Hydrol.*
1003 *Process.*, 14(8), 1449–1464, doi: 10.1002/1099-1085(20000615)14:8<1449::AID-
1004 HYP993>3.0.CO;2-7.

1005 Wiles, G., D'Arrigo, R., Villalba, R., Calkin, P., and Barclay, D.J., (2004), Century-scale
1006 solar variability and Alaskan temperature change over the past millennium, *Geophys.*
1007 *Res. Lett.* 31, L15203, doi: 10.1029/2004GL020050.

1008 Zander, P.D., Kaufman, D.S., Kuehn, S.C., Wallace, K.L., and Anderson, R.S., (2013), Early
1009 and late Holocene glacial fluctuations and tephrostratigraphy, Cabin Lake, Alaska, *J. Quat.*
1010 *Sci.*, 28, 761–771, doi: 10.1002/jqs.2671

1011 Zhang, Y., Renssen, H., Seppä, H., and Valdes, P.J., (2017), Holocene temperature
1012 evolution in the Northern Hemisphere high latitudes–Model-data comparisons, *Quat. Sci.*
1013 *Rev.*, 173, 101–113, doi: 10.1016/j.quascirev.2017.07.018.

1014 **Author contributions**

1015 D.S.K was project PI, led the fieldwork and retrieved the sediment cores. D.S.K., H.L.B,
1016 H.J.S., A.C.G.H. and M.J.L developed the study concept. H.L.B conducted the research,
1017 sample preparation, SEM, diatom and statistical analyses, interpreted the results, produced
1018 the figures, and wrote the original manuscript. H.J.S performed the FTIR and diatom isotope
1019 measurements. D.S.K. and A.L.H. critically revised the original manuscript, and together
1020 with H.M. and J.W. provided technical advice and comments. M.J.L. supervised the diatom
1021 isotope measurements and undertook the isotope corrections. H.J.S., A.C.G.H. and M.J.L.
1022 provided comments and minor editorial revisions. All authors approved the final manuscript.

1023

1024 **The authors declare no competing financial interests.**